Dear reviewer 2,
thank you for taking the time and reviewing our paper again!

Comments

- NAT sedimentation: The results shown in Höpfner et al. and Eckermann et al. can't resolve the HCl problem: The detected NAT PSCs are at the edge of the vortex, but the HCl discrepancy shows up in the core of the vortex (see the plots attached to my last reply). Note that the -5 K change to HCl solubility is applied to STS droplets in my model, while you are talking about 5 K temperature fluctuations in mountain waves causing large NAT particles to sediment. So, I don't know what you mean if you write "So in this case the sensitivity study with a 5 K temperature shift is reasonable." It would be reasonable if I would remove HCl by sedimenting NAT particles, which I don't do. The distance that STS droplets will sediment is not large, and the uptake of HCl by STS will be reversible.

  For the reasons mentioned above, I does not make sense to discuss the above references in my paper, since it is quite obvious that NAT sedimentation at the edge of the vortex will not be the solution and that the magnitude of my temperature bias is also not explained by this. Note that there already was (and is) a short discussion of sedimentation of HCl as a possible reason for the discrepancy on page 37, lines 19–20.

  It is unclear to me how large the amount of HCl would be that is removed by NAT particles, but the removed HCl has to be set free again at a lower altitude, which probably should be visible in the measurements. In addition, I would expect then that there is some temporal correlation between the decrease in HNO3 and HCl, which is not observed (see Phd. thesis Wegner), although this picture may be too simple. These questions can probably only be answered ultimately by actually modelling the uptake of HCl by NAT and how it is set free again, which is however outside the scope of this paper.

- Corrected and adjusted: You are right, it is better to speak of an adjustment of the HCl solublity, I don't know if it is a correction. However, as far as I refer to the HCl mixing ratios, it is correct to speak of a correction (if you have faith in the MLS measurements). Changed the manuscript along these lines.

1

Dear reviewer 3,
thank you for taking the time and reviewing our paper again!

Substantive comments

- Supplement: Added references to the figures in the supplement where applicable.

- Interhemispheric differences in peak ClOx values: You are right, there is an underestimation of ClO in ATLAS in the southern hemisphere in 2006 of about 0.2–0.4 ppb (estimate based on line plots along satellite paths not shown in the supplement). This is consistent with an overestimation of HCl of the same order of magnitude in the southern hemisphere. This somehow escaped my attention. I have changed the discussion and the conclusions accordingly.

- HCl model/measurement discrepancy (HCl December): Chlorine activation starts too early in December 2004, peak ClO values are overestimated by ATLAS compared to MLS by up to 0.5 ppb on 15 December (estimated from line plots along the satellite tracks not shown in the supplement). The difference between the "corrected" and "uncorrected" run is mainly caused by the changed γ values of the reactions, there is almost no HCl in the liquid phase in December 2004. Added discussion of this to section 6.

- HCl model/measurement discrepancy (Errors in subsidence): The sentence at page 37, lines 14–15 is phrased quite carefully and as it is formulated, it is a robust assumption (if you ignore measurement errors, this is just a basic fact, since changes in a chemically conserved species can only be caused by transport or mixing). I would like to leave the discussion in the paper as is and will discuss the reasons here.

  Of course, it cannot be excluded that errors in subsidence and errors in mixing combine in an unfortunate way that still leads to a good agreement of model and measurements for N2O, but cause errors in other species. But that seems unlikely to me.

  Unfortunately, this is not easy to prove: While it is relatively easy to disentangle the two effects in the model (i.e. for the ECMWF world) by introducing a vortex tracer and a tracer for potential temperature, it is not as easy for the real world, because you can't observe heating rates or mixing directly. A single conserved tracer like N2O does obviously not contain enough information to disentangle the two effects. Maybe it is possible by looking at two or more conserved tracers and to obtain some values for the strength of mixing and subsidence to compare with the model from that, but I am not sure that this has ever been tried and this is for sure a study of its own.

  Regarding the accumulation of errors: I don't think that the accumulation of errors in one species (N2O) can be small, while it is large in another

species (HCl), as long as the vertical gradients do not combine in an unfortunate way. Assuming for a moment that we just have subsidence and no mixing, the difference in N2O between ATLAS and MLS can be converted to a vertical distance by the vertical gradient in N2O, and that can in turn be converted to the expected change in Cly or HCl by looking at the vertical gradient in these species. There is no indication that the small differences in N2O between ATLAS and MLS (which are still inside the accuracy of MLS) can cause a change of more than 1 ppb in HCl.

- HCl model/measurement discrepancy (Conclusions): Added a paragraph to the conclusions discussing the HCl discrepancy.

- Model validation O3: No, we have no explanation for that. There has been no thorough validation of the model in extrapolar latitudes so far, since it is mainly used for polar studies. The discrepancy also depends on the year and is more pronounced in some years than in others.

- Model validation ClONO2: You are right, this needs to be phrased more carefully. Note however that the measurements in June only reach up to 60 degrees south, while the problem shows up south of 60 degrees south in the following months. Ignoring transport for a moment, the figures for June don't tell much about the discrepancy that shows up later. But I agree that the problem is possibly also caused by chemistry. What cannot be seen in the plots very well is that the difference between ATLAS and ACE-FTS is up to 0.3 ppb in June (the color scale is not optimal, I have additional difference plots here that are not shown in the supplement).

- Figure changes: I am sorry that I forgot to mention in my reply that I slightly changed the averaging applied in the figures to obtain values for days where I did not have a value so far. This was applied both to the plots in the paper and in the supplement. In the old plots, I first calculated a vortex average (with additional conditions like day, night or vortextracer larger than 0.7 and a minimum number of points required) for every output file of the model, which are at 00 h UTC and 12 h UTC. Then, the values for 00 h UTC and 12 h UTC were averaged to obtain a mean value for the day. Unfortunately, sometimes one of the 00 h UTC or 12 h UTC averages did not contain enough points, while the other did. In these cases I did not plot a value. Now, I first collect all of the points from the 00 UTC and 12 UTC output file into one dataset and then calculate the average (which also weights all points equally, which was not strictly the case in the old approach).

Minor points

- P2, L3: Done.

- P2, L21-22: Done.

- P3, L1: Done.

- P5, L14: Done.

- P6, L22: Done.

- P12, L10: Done.

- P12, L15: Done.

- P13, L16: Done.

- P14, L15–18: Done as suggested.

- P17, L5: Done.

- P18, L6: Done.

- P18, L7: Done.

- P19, L5: Done.

- P19, L6: Since this is widely known, I think it is ok to give no reference here.

- P19, L12: Done.

- P21, L14-16: Done.

- P21, L23: Done.

- P21, L24: Done.

- P21, L26: Done.

- P21, L30: Deleted "2006". Added "to the beginning of October", since ClOx drops very quickly at the start of October.

- P23, L18: Done.

- P24, L1–4: Replaced "initially" by "December" and "May".

- P25, L29: Corrected.

- P29, L9: Done.

- P29, L26: Done.

- P31, L6: Done.

- P32, L6: Done.

- P32, L16: Done.

- P33, L2: Done.

- P33, L5-7: Done. I assume you mean "altitudes" and not "latitudes".

- P33, L12: Done.

- P33, L25: Done.

- P33, L27: Done.

- P33, L29–30: Done.

- P34, L2–3: Done. You probably mean Santee et al. (2008) and not Manney et al. (2011)?

- P34, L13: Done.

- P34, L17: Done.

- P34, L22: Done.

- P35, Figure 21 caption: Done.

- P37, L11: Done.

- P37, L32: Done.

- P38, L2: Done.

- P38, L7: In Brakebusch et al. and Solomon et al. the temperature bias was only introduced in the heterogeneous chemistry module and not in the complete model. I have now added this information to the paper. The bias introduced in these papers is -1.5 K and considerably lower than the bias of -5 K used by me. One of the reasons for the difference may be that the reaction rates of the heterogenous reactions are changed directly via their temperature dependence in the approach by Brakebusch et al. which is not the case in my approach. Rephrased the discussion here to reflect this.

- P38, L8–9: Done. Added a remark that there remains an HCl overestimation in ATLAS of 0.2 to 0.4 ppb in the southern hemisphere, consistent with the discrepancy between MLS ClO and ATLAS ClO.

- P38, L12: Corrected.

- P38, L24: Done.

- P38, L29: Done.

- P39, L12: Done.

- P39, L18-19: Done.

A quantitative analysis of the reactions involved in stratospheric ozone depletion in the polar vortex core

Ingo Wohltmann[1], Ralph Lehmann[1], and Markus Rex[1]

[1]Alfred Wegener Institute for Polar and Marine Research, Potsdam, Germany

Correspondence to: I. Wohltmann (ingo.wohltmann@awi.de)

Abstract. We present a quantitative analysis of the chemical reactions involved in polar ozone depletion in the stratosphere, and of the relevant reaction pathways and cycles. While the reactions involved in polar ozone depletion are well known, quantitative estimates of the importance of individual reactions or reaction cycles are rare. In particular, there is no comprehensive and quantitative study of the reaction rates and cycles averaged over the polar vortex under conditions of heterogeneous chemistry so far. We show time series of reaction rates averaged over the core of the polar vortex in winter and spring for all relevant reactions and indicate which reaction pathways and cycles are responsible for the vortex-averaged net change of the key species involved in ozone depletion, that is ozone, chlorine species (ClO_x, HCl, $ClONO_2$), bromine species, nitrogen species (HNO_3, NO_x) and hydrogen species (HO_x). For clarity, we focus on one Arctic winter (2004/2005) and one Antarctic winter (2006) in a layer in the lower stratosphere around $54\,hPa$, and show results for additional pressure levels and winters in a supplement. Mixing ratios and reaction rates are obtained from runs of the ATLAS Lagrangian Chemistry and Transport Model (CTM) driven by ECMWF ERA Interim reanalysis data. An emphasis is put on the partitioning of the relevant chemical families (nitrogen, hydrogen, chlorine, bromine and odd oxygen) and activation and deactivation of chlorine.

1 Introduction

After the discovery of the ozone hole (Farman et al., 1985), the chemistry of polar ozone depletion in the stratosphere has been the subject of ongoing research for the last 30 years (see e.g. articles, review papers and text books by Solomon et al., 1986, Wayne et al., 1995, Portmann et al., 1996, Brasseur et al., 1999, Solomon, 1999, Brasseur and Solomon, 2005, WMO, 2011, Müller, 2012, Solomon et al., 2015). In general, the chemistry of polar ozone depletion is understood very well (see e.g. the recent overview in Müller, 2012, or von Hobe et al., 2013). Remaining issues, such as uncertainties in the formation pathways of Polar Stratospheric Clouds (PSCs) or uncertainties in the contribution of the different cloud types to chlorine activation (e.g. Lowe and MacKenzie, 2008; Peter and Grooß, 2012; Wohltmann et al., 2013), do not pose a serious challenge to the generally accepted basic theory.

While the reaction pathways and reaction cycles that are involved in ozone depletion are well known (e.g. Portmann et al., 1996; Solomon, 1999; Müller, 2012), quantitative estimates of the importance of single reactions or reaction cycles are rare, and are limited to case studies or certain aspects of the chemical system (e.g. Portmann et al., 1996; Grenfell et al., 2006; Frieler et al., 2006) or apply mainly to conditions undisturbed by heterogeneous chemistry (e.g. Brasseur and Solomon, 2005).

Here, we give a comprehensive overview of the temporal evolution of the vortex-averaged reaction rates and mixing ratios and associated reaction pathways and cycles for one Arctic winter (2004/2005) and one Antarctic winter (2006) in a layer in the lower stratosphere around $54\,\mathrm{hPa}$. Results for additional winters and pressure levels can be found in a supplement and are summarized in the paper. Vortex-averaged mixing ratios and reaction rates are obtained from runs of the Lagrangian
5 (trajectory-based) ATLAS Chemistry and Transport Model (Wohltmann and Rex, 2009; Wohltmann et al., 2010). Since results cannot be based on direct observations due to a lack of measurements of the mixing ratios of minor species and reaction rates, only a model-based approach is feasible. The most important model parameters that influence the vortex-averaged rates are the initial mixing ratios, the laboratory measurements of the rate coefficients of the reactions (taken from Sander et al., 2011) and the meteorological data that drive the model, which are taken from the European Centre for Medium-Range Weather Forecasts
10 (ECMWF) ERA Interim reanalysis (Dee et al., 2011). A detailed study of the uncertainties is outside the scope of this paper, but some of the major uncertainties will be noted. For a study of the uncertainties, see e.g. Kawa et al. (2009).

Reasonable agreement of the modeled and observed mixing ratios for many species gives us confidence that our results represent the real atmosphere well in most cases (see the basic validation against observations in Section 6 and extensive additional comparisons of the model to measurements in the supplement). There was however a significant overestimation of
15 HCl compared to measurements in our original model runs, which has also been observed in other models like SD-WACCM (Brakebusch et al., 2013; Wegner, 2013; Solomon et al., 2015) or MIMOSA-CHIM (Kuttippurath et al., 2015). Interestingly, the SLIMCAT CTM shows a discrepancy of the same order of magnitude, but with opposite sign in a recent publication (Santee et al., 2008).

Hence, we consider the differences in HCl between models and observations as "state-of-the-art" in current CTMs and apply
20 an empirical correction to bring the HCl mixing ratios in closer agreement to observations. The correction is based on changing the HCl solubility, which is a possible cause for this discrepancy. This introduces some uncertainty in our results, which ~~are~~ is explored in Section 6 and by comparisons to the uncorrected runs shown in the supplement. However, a detailed discussion of this important issue would deserve its own study.

While it is easy to identify the gross production or loss of a species by single reactions, it is difficult to identify what causes
25 the net loss or production of a species (e.g. Lehmann, 2002). Often, the reactions that directly produce or remove a species of interest are part of a complicated chain of reactions, frequently involving reaction cycles. Many of these cycles will consume as much of a species as they produce (null cycles, equilibria), others will lead to a net loss of the species (loss cycles). Numerous loss cycles in the stratosphere are catalytic cycles, i.e. they destroy the species of interest with the help of another species that is constantly recycled in the loss cycle. To complicate things further, cycles may share species and reactions. Hence, it is of
30 crucial importance to know the reaction cycles and pathways in the chemical system to actually understand the underlying reasons for the loss or production of a species, and these relationship are discussed in the following.

In Section 2, the methods and the model are introduced. The section contains a description of the ATLAS model and the setup of the runs and explains the method to obtain vortex-averaged reaction rates. In Section 3, we give an overview of the typical evolution of polar ozone chemistry in winter to provide a foundation for the following discussion. Section 4 discusses
35 reactions and partitioning sorted by chemical families, that is nitrogen, hydrogen, chlorine, bromine and oxygen compounds.

Section 5 explores ~~in~~ how far the results can be generalized to other years. Section 6 discusses the HCl discrepancy and gives a short discussion of validation of other species with observations. Section 7 contains the conclusions.

Results of this study are extensively used in a companion paper (Wohltmann et al., 2017) to develop a fast model for polar ozone chemistry.

2 Model and methods

2.1 Model overview

ATLAS is a global Chemistry and Transport Model (CTM) based on a Lagrangian (trajectory-based) approach. A detailed description of the model can be found in Wohltmann and Rex (2009) and Wohltmann et al. (2010). Updates to the chemistry module and polar stratospheric cloud module are described in Wohltmann et al. (2013). The model includes a gas-phase stratospheric chemistry module, heterogeneous chemistry on polar stratospheric clouds, a particle-based Lagrangian denitrification module and a dehydration parameterization. The chemistry module comprises 47 active species and more than 180 reactions. Absorption cross sections and rate coefficients are taken from recent JPL recommendations (Sander et al., 2011). In addition to the binary background aerosol, the model simulates three types of Polar Stratospheric Clouds, that is supercooled ternary $HNO_3/H_2SO_4/H_2O$ solutions (STS), solid clouds composed of nitric acid trihydrate (NAT), and solid ice clouds.

2.2 Model setup

Model runs are driven by meteorological data from the ECMWF ERA Interim reanalysis (Dee et al., 2011). The initial horizontal model resolution is $150\,km$. The runs use the hybrid pressure-potential temperature coordinate of the model, which is a pure potential temperature coordinate above $100\,hPa$. The vertical range of the model domain is $350\,K$ to $1900\,K$. Vertical motion is driven by diabatic heating rates from ERA Interim. Two model runs are started, one for the northern hemispheric winter, and one for the southern hemispheric winter. The run for the northern hemisphere starts on 1 October 2004 and ends on 31 March 2005. The run for the southern hemisphere starts on 1 April 2006 and ends on 30 November 2006. Model data before 15 November 2004 or 1 May 2006 are not used for analysis to allow for a spin up of the mixing in the model and for a sufficiently stable vortex in the northern hemisphere. Results for two additional winters (2009/2010 in the northern hemisphere and 2011 in the southern hemisphere) are only shown in the supplement.

The number density of NAT particles in the runs is set to $0.1\,cm^{-3}$, the number density of ice particles is set to $0.01\,cm^{-3}$ and the number density of the ternary solution droplets is set to $10\,cm^{-3}$. A supersaturation of HNO_3 over NAT of 10 (corresponding to about $3\,K$ supercooling) is assumed to be necessary for the formation of the NAT particles. A detailed discussion of the rationale behind these choices can be found in Wohltmann et al. (2013). For ice particles, a supersaturation of 0.35 is assumed based on Microwave Limb Sounder (MLS) satellite measurements of H_2O (Waters et al., 2006) and ECMWF temperatures.

3

The treatment of conditions where both NAT and STS clouds are allowed to form has changed compared to Wohltmann et al. (2013). Since mixed NAT/STS clouds are commonly observed (e.g. Pitts et al., 2011), they can now form in the model to allow for a more realistic behaviour, see Nakajima et al. (2016) for details.

The settings for the polar stratospheric cloud parameterizations largely favor the formation of liquid clouds (binary liquids and STS clouds) over the formation of NAT clouds and activation of chlorine predominantly occurs on liquid clouds in the model runs.

The Lagrangian particle model is used to simulate the nucleation, growth, sedimentation and evaporation of large NAT particles. These particles are formed with a nucleation rate of 7.8×10^{-6} particles per h and cm^3 and an initial radius of 0.1 µm, wherever a supersaturation of 10 for HNO_3 is exceeded. Dehydration by falling ice particles is simulated by a simple algorithm that irreversibly removes all ice above a given supersaturation, which is set to 0.7 here (note that the value 0.35 given above is only used in the chemistry module, the value in the dehydration module is set separately).

H_2O, N_2O, HCl, O_3, CO and HNO_3 are initialized from all measurements of the MLS instrument performed during 1 November 2004 and 1 May 2006 for the northern and southern hemispheres, respectively. CH_4 is initialized from a monthly mean HALOE (Halogen Occultation Experiment) climatology (mean of the years 1991–2002) as a function of equivalent latitude and pressure (Grooß and Russell III, 2005). NO_x is initialized from the monthly mean HALOE data set by putting all NO_x into NO_2. $ClONO_2$ is calculated as the difference between Cl_y and HCl. Cl_y is taken from a Cl_y-N_2O tracer-tracer correlation from ER-2 aircraft and Triple balloon data (Grooß et al., 2002). As in Wohltmann et al. (2013), we increase the amount of $ClONO_2$ by 10 % at the expense of HCl, see the discussion there. $BrONO_2$ is assumed to contain all Br_y, which is taken from a Br_y-CH_4 relationship from ER-2 aircraft and Triple balloon data in Grooß et al. (2002). All Br_y values are scaled with a constant factor to give maximum values of 19.9 ppt.

2.3 Production and loss rates

Reaction rates are calculated for every reaction separately in the ATLAS model. For this purpose, one artificial species per reaction is introduced to the model, which is produced at the same rate as the other products of the reaction. For instance, a reaction of the type

$$A + B \rightarrow C + D$$

is modified to

$$A + B \rightarrow C + D + P$$
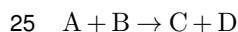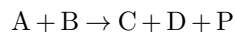
where P is an artificial product species. The mixing ratio of the artificial product species is reset to zero every 24 hours. This way, P directly gives the 24 h averaged rates of production of the species C and D by this reaction and the 24 h averaged loss rates of the species A and B. The 24 h time period is used to capture the diurnal cycle of the photochemically active species. For technical reasons, heterogeneous reaction rates with the same chemical equation, but on different surface types are added together in a single reaction rate.

2.4 Vortex averages

Production and loss rates are averaged over all air parcels of the model inside the polar vortex that are situated in a layer between $61.3\,\mathrm{hPa}$ and $47.4\,\mathrm{hPa}$. The logarithmic mean level of this layer is at $54\,\mathrm{hPa}$. The vortex edge is assumed to be situated at the $36\,\mathrm{PVU}$ contour of modified potential vorticity (PV) in the northern hemisphere and at the $-36\,\mathrm{PVU}$ contour in the southern hemisphere. Modified PV is calculated from the potential vorticity field of the ERA Interim reanalysis according to Lait (1994), with $\theta_0 = 475\,\mathrm{K}$. The supplement shows results for the additional pressure levels 32 hPa, 42 hPa and 70 hPa.

In order to obtain a more consistent picture of the ozone chemistry in the vortex, we exclude air parcels that experience a too high amount of mixing with extra-vortex air during the course of the model run. This basically limits our results to the core of the vortex. For that purpose, we initialize a "vortex tracer" as an artificial chemical species near the start of the model run (15 November in the northern hemisphere, 1 May in the southern hemisphere), which is set to 1 inside the vortex and to 0 outside the vortex. The vortex tracer is then transported and mixed like any other species in the model and can take any value between 0 and 1. We only include in the vortex mean those parcels for which the vortex tracer has a value greater than 0.7. This value was chosen as a compromise between obtaining a sufficient number of trajectories for averaging and a set of trajectories that is chemically sufficiently ~~homogenous~~homogeneous.

Without the vortex tracer, analysis would get much more complicated. An example may illustrate this: In the southern vortex, air masses rich in NO_y are mixed into the edge region of the vortex during the course of the winter, while in the core of the vortex, air masses are depleted of nitrogen species due to denitrification. This leads not only to differences in mixing ratios of the nitrogen species over the vortex, but also to different reactions being important in different parts of the vortex. For example, while very low ozone values are reached in the core of the vortex since deactivation into $ClONO_2$ is hindered, ozone values at the edge are higher and chlorine is also deactivated into $ClONO_2$ ($ClONO_2$ "collar", see e.g. Douglass et al., 1995).

2.5 Different air masses

The $54\,\mathrm{hPa}$ level is not a material surface and we look at different air masses at different points of time, due to mixing, the movement of the isentropes relative to the pressure level and the additional sinking of the air masses relative to isentropes due to diabatic cooling. A similar caveat applies to the definition of the vortex edge. As a consequence of these transport effects, the temporal derivative of the vortex-averaged mixing ratio of a chemical species may deviate from the vortex-averaged chemical net change of this species.

Unfortunately, it is difficult to look at the same air mass over the course of several months, since an air mass with a well defined extent at the beginning of the winter will completely lose its identity due to mixing and transport during the course of the winter.

2.6 Equilibria

In many cases, two species X and Y with short lifetimes are in a fast equilibrium with each other, and will not change their mixing ratios if the external conditions do not change. For example, consider two fast reactions of the form

$$X + Z_1 \rightarrow Y + \ldots$$

5   $Y + Z_2 \rightarrow X + \ldots$
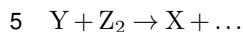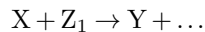
Then, assuming that the change of the mixing ratios is zero

$$\frac{d[X]}{dt} = -k_1[X][Z_1] + k_2[Y][Z_2] = 0 \tag{1}$$

where $[X]$ is the concentration of X and k_1 and k_2 are the reaction coefficients, we obtain equilibrium conditions like

$$\frac{[X]}{[Y]} = \frac{k_2[Z_2]}{k_1[Z_1]}. \tag{2}$$

10   Similar equations can be derived for more complex reaction systems. We use the equilibrium conditions in the following not only to show relationships between mixing ratios of different species, but also to determine the reactions involved in an equilibrium: For a given set of species, we start with a small set of reactions involved in the equilibrium derived from the vortex-averaged reaction rates, and calculate the mixing ratios of the species from the equilibrium conditions. Then, we compare these mixing ratios with the mixing ratios in the output of the model. If the mixing ratios determined by the two methods do not

15   agree with each other, we add reactions until we reach good agreement with a set of reactions as small as possible.

3 Short overview of the chemical evolution

The evolution of the chemistry of polar ozone depletion can be divided into several phases (first defined by Portmann et al., 1996). For orientation, Figure 1 shows the evolution of temperature and sunlight in both hemispheres.

After the polar vortex forms in late autumn and early winter in response to the cooling of the atmosphere in the beginning of

20   polar night, air masses in the vortex are well isolated from mid latitudes (e.g. Solomon, 1999). In the first phase in early winter, chlorine, the main player in the chemistry of lower stratospheric ozone depletion, is present mainly in the form of species that do not directly contribute to ozone depletion. These passive reservoir gases are mainly HCl and $ClONO_2$ (e.g. Solomon, 1999). Chemical activity is low due to the lack of sunlight in the polar night. This period lasts from the forming of the vortex until the first polar stratospheric clouds form.

25   In the second phase, HCl and $ClONO_2$ are transformed from passive reservoir gases to Cl_2 through heterogeneous reactions on the surface of polar stratospheric clouds (e.g. Solomon et al., 1986), which condense when temperatures in the polar night get cold enough. A second effect of the clouds can be the removal of large quantities of HNO_3 and H_2O by sedimentation (denitrification and dehydration, e.g. Toon et al., 1986, Fahey et al., 1990), which can prolong ozone loss later in spring (e.g. Portmann et al., 1996). In the model setup used here, activation predominantly occurs on liquid STS clouds and only to a lesser
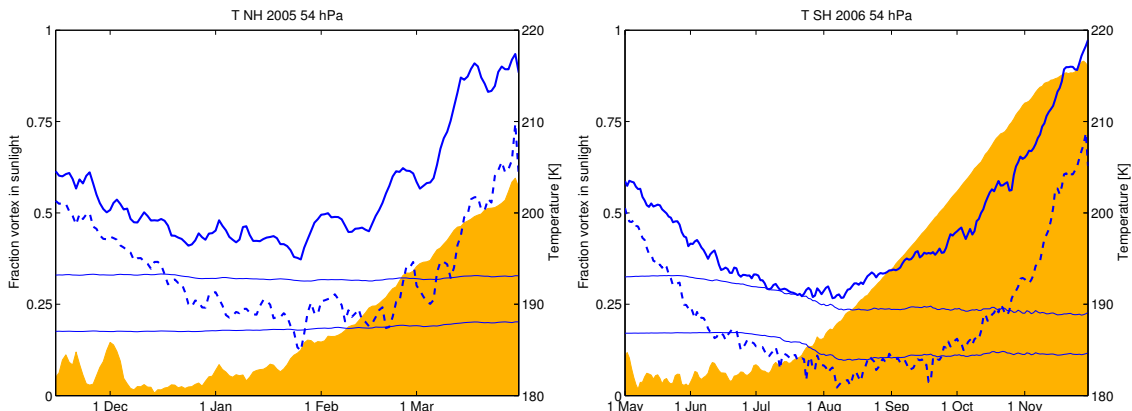
Figure 1. Vortex-averaged temperature (blue), vortex minimum temperature (dashed blue) and fraction of the vortex in sunlight (yellow) for the Arctic winter 2004/2005 (left) and the Antarctic winter 2006 (right) at 54 hPa. The upper thin blue line shows the threshold temperature for the formation of NAT clouds used in the model (based on vortex mean mixing ratios and considering supersaturation), and the lower thin blue line shows the same for ice clouds. The vortex tracer criterion described in the text was not applied (in contrast to all other figures).

part on solid NAT clouds. Unfortunately, observations of PSCs are not detailed enough to sufficiently constrain the ratio of activation on STS versus NAT clouds, and there is also uncertainty in other parameters like size distribution, number densities and required supersaturation. However, chlorine activation and ozone loss are robust quantities with respect to most changes in PSC parameterizations (Wohltmann et al., 2013).

5   The third phase starts when sunlight comes back, enabling catalytic cycles to destroy ozone in large quantities. Cl_2 is transformed to Cl and ClO by photolysis. Then ozone is removed mainly by the catalytic ClO dimer cycle and the catalytic ClO–BrO cycle (e.g. Solomon, 1999). The second cycle makes ozone destruction sensitive to the amount of bromine and to bromine chemistry. At the same time, reactions that deactivate active chlorine and that are dependent on sunlight gain importance. Hence, there is a constant competition between activation and deactivation in this phase, as long as it is cold
10   enough (e.g. Portmann et al., 1996; Solomon et al., 2015).

In the fourth phase, when temperatures rise in spring and PSCs evaporate, chlorine is deactivated into the reservoir gases again and ozone loss significantly decreases.

4   Budgets of the chemical families and chemical evolution arranged by families

4.1   Nitrogen species

15   NO_y is defined as the sum of all nitrogen containing species except for the long-lived source gas N_2O, which is the source of all other nitrogen species in the stratosphere. N_2O has both natural and anthropogenic sources in the troposphere (e.g. WMO, 2011; Montzka, 2012). Figure 2 shows the partitioning of NO_y at 54 hPa. The majority of NO_y is in the form of HNO_3 in
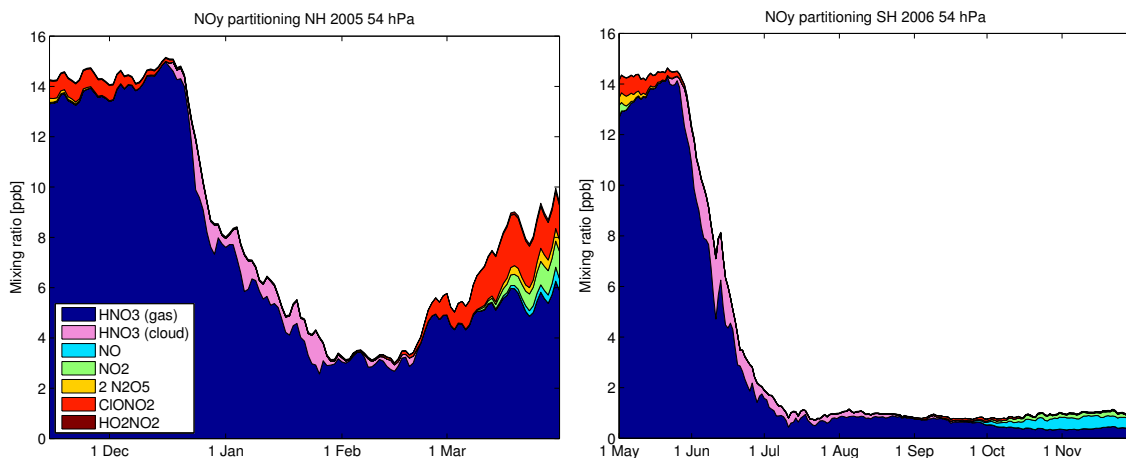
Figure 2. Vortex-averaged partitioning of NO_y species for the Arctic winter 2004/2005 (left) and the Antarctic winter 2006 (right) at $54\,hPa$. Species NO_3, $BrONO_2$, $ClNO_2$ and N are not shown due to their small mixing ratios.

the considered altitude range. This is due to the fact that removal of HNO_3 by photolysis and OH is not very efficient at these altitudes. The initial level of HNO_3 is about 13 to $14\,ppb$ in both hemispheres and the initial NO_y is about $1\,ppb$ higher. Figure 2 shows that the mixing ratio of HNO_3 (and NO_y) declines to about $3\,ppb$ in February 2005 in the northern hemisphere and increases again in March due to transport (see Figure 3, which shows that the rate of change by chemistry is small in

5   this time period). In contrast, HNO_3 decreases to about $0.5\,ppb$ (with NO_y at $1\,ppb$) in the southern hemisphere after June 2006. The rate of change of HNO_3 is not dominated by chemical changes, but by denitrification, i.e. the irreversible removal of HNO_3 by sedimenting cloud particles (e.g. Toon et al., 1986; Fahey et al., 1990), as shown in Figure 3. Denitrification is much more severe in the southern hemisphere due to the lower temperatures (see Figure 1, e.g. Solomon, 1999), leaving almost no NO_y. The amount of NO_y present in the other important nitrogen reservoir $ClONO_2$ is limited by the mixing ratio of Cl_y (less

10   than $3.5\,ppb$). Thus, $ClONO_2$ never contributes more than about $25\,\%$ to NO_y. The supplement shows that NO_y increases with height from $10\,ppb$ at $70\,hPa$ to $18\,ppb$ at $32\,hPa$, but that the majority is always in the form of HNO_3 (Figures 2, 26, 50, 74 of the supplement).

NO_x is defined as the sum of the short-lived and reactive species NO, NO_2, NO_3 and $2\,N_2O_5$, which only form under sunlit conditions from the longer lived HNO_3. Only a small part of NO_y is in the form of NO_x under sunlit conditions, typically less

15   than $1.5\,ppb$ in the northern hemisphere and less than $0.5\,ppb$ in the southern hemisphere at $54\,hPa$. The supplement shows that NO_x increases from about $0.5\,ppb$ at $70\,hPa$ to about $2.5\,ppb$ at $32\,hPa$ in the northern hemisphere due to increasing radiation (Figures 5, 29 of the supplement). For the following discussion, it is reasonable to define an "extended" NO_x, which also includes $ClONO_2$ (and, much less importantly, $BrONO_2$ and HO_2NO_2), since these species are in very fast equilibria with the "classical" NO_x species under sunlit conditions.
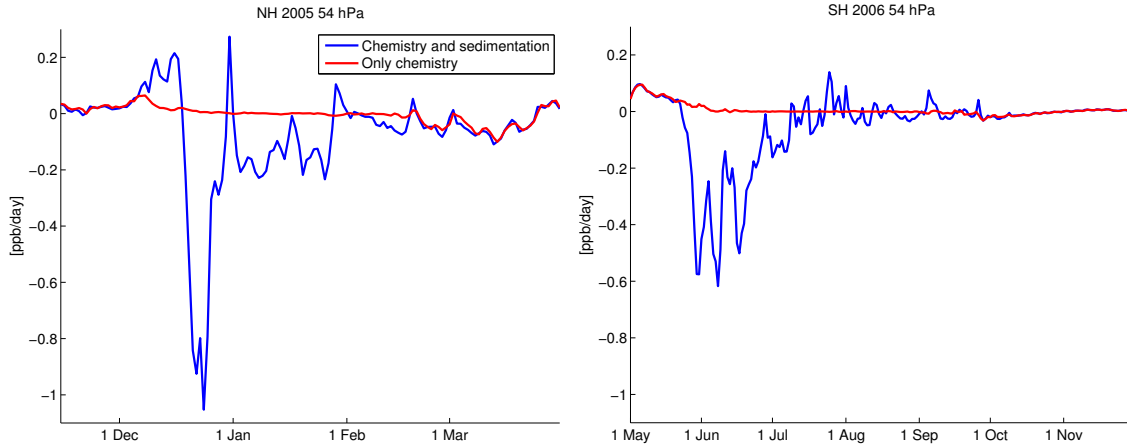
8

Figure 3. Vortex-averaged net chemical reaction rate of HNO_3 (red) for the Arctic winter 2004/2005 (left) and the Antarctic winter 2006 (right) at $54\,\mathrm{hPa}$ and sum of the vortex-averaged change by sedimentation and the net chemical reaction rate (blue).
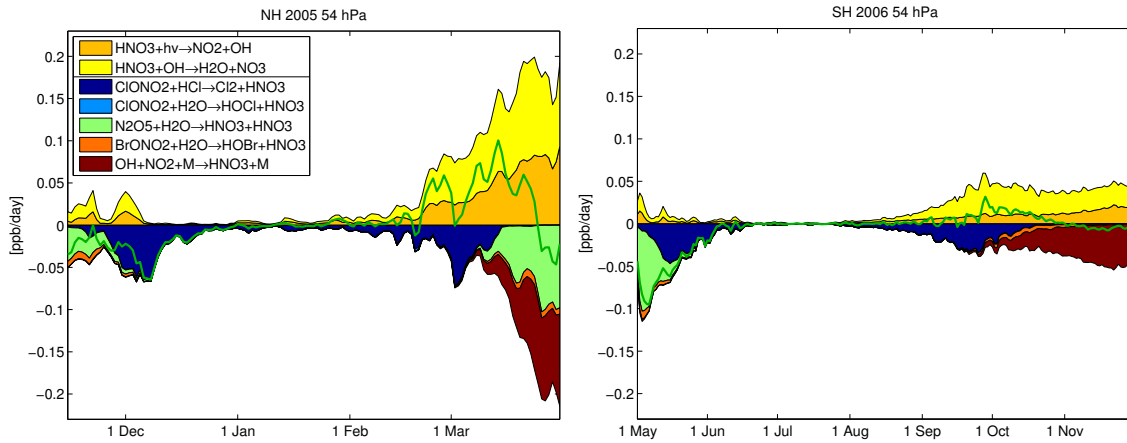

Figure 4. Vortex-averaged chemical reaction rates of reactions changing extended NO_x ($NO + NO_2 + NO_3 + 2\,N_2O_5 + ClONO_2 + BrONO_2 + HO_2NO_2$) for the Arctic winter 2004/2005 (left) and the Antarctic winter 2006 (right) at $54\,\mathrm{hPa}$. Production reactions are shown positive and are separated by a line in the legend from the loss reactions, which are shown negative. The net change of extended NO_x is shown as a green line. Reactions with rates which cannot be distinguished from the zero line at plot resolution are not shown.

9

The extended NO_x mixing ratios can be changed by a number of reactions. Vortex-averaged reaction rates of these reactions for the northern and southern hemisphere are shown in Figure 4. Extended NO_x is almost exclusively produced from HNO_3 under sunlit conditions by photolysis and reaction with OH

$$HNO_3 + h\nu \rightarrow NO_2 + OH \tag{R1}$$

5

$$HNO_3 + OH \rightarrow H_2O + NO_3 \tag{R2}$$

see e.g. Portmann et al. (1996). The OH reaction contributes about 60 %–80 % of the production (cf. Figure 7 in Portmann et al., 1996). Extended NO_x is lost to HNO_3 mainly by the heterogeneous reactions

$$N_2O_5 + H_2O \rightarrow HNO_3 + HNO_3 \tag{R3}$$

10

$$ClONO_2 + HCl \rightarrow Cl_2 + HNO_3 \tag{R4}$$

and by the gas-phase reaction

$$OH + NO_2 + M \rightarrow HNO_3 + M. \tag{R5}$$

The reaction $N_2O_5 + H_2O$ proceeds on the background aerosol, not only when polar stratospheric clouds are present. When
15   sunlight comes back to the vortex in spring, reactions R1–R2 are not in equilibrium with R3–R5 and net production of extended NO_x from HNO_3 occurs (e.g. Portmann et al., 1996). Due to the denitrified conditions in the southern hemisphere, much less NO_x is produced there (e.g. Douglass et al., 1995). While the rates of the reactions changing extended NO_x increase by a factor of 4 from 70 hPa to 32 hPa (see in the northern hemisphere (Figures 4, 28 of the supplement), the relative importance of the reactions does not change.

20   Note that the introduction of an extended NO_x does not work very well under polar night conditions, since $ClONO_2$ is not in equilibrium with the classical NO_x then, which can be seen in the fact that extended NO_x is lost in polar night due to heterogeneous reaction of $ClONO_2$, although no NO or NO_2 is present.

Figure 5 shows the partitioning of extended NO_x during daytime and at night. Daytime averages are defined over the parts of the vortex where the solar zenith angle is smaller than $80°$ and nighttime averages are defined over parts of the vortex where
25   the solar zenith angle is larger than $100°$ (note that this means that the areas for the daytime average and the nighttime average may not be coincident). Except for early winter, NO_x proper is only present in appreciable quantities after the start of March 2005 or October 2006 in the northern and southern hemispheres, respectively. During daytime, the partitioning between NO and NO_2 is so fast that steady state conditions can be assumed (e.g. Douglass et al., 1995). The three reactions that determine the equilibrium are
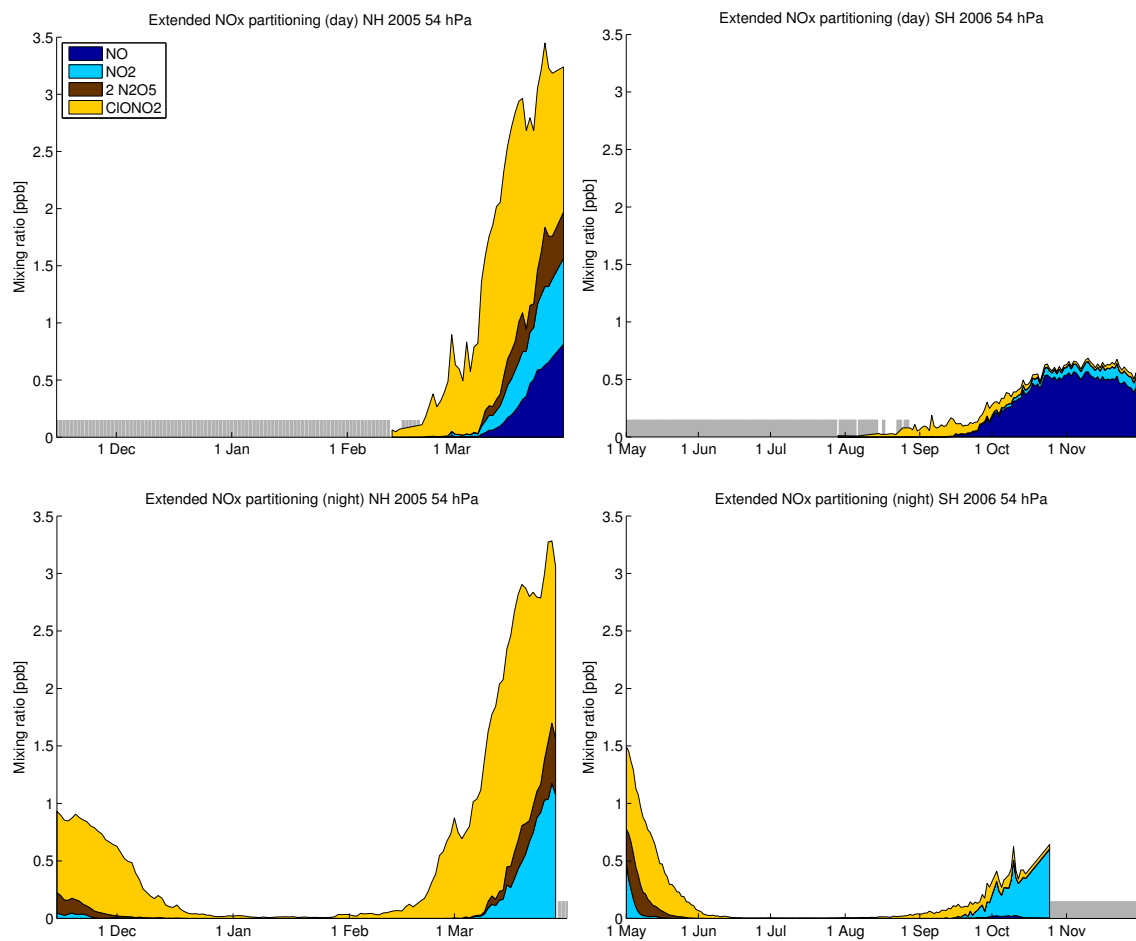
30   $$O_3 + NO \rightarrow NO_2 + O_2 \tag{R6}$$

Figure 5. Vortex-averaged partitioning of extended NO_x species for the Arctic winter 2004/2005 (left) and the Antarctic winter 2006 (right) at $54\,hPa$. Top row: Daytime averages (parts of the vortex where the solar zenith angle is smaller than $80°$). Bottom row: Nighttime averages (parts of the vortex where the solar zenith angle is larger than $100°$). Days without sufficient data for averaging are not shown (grey bars).

$$\mathrm{ClO + NO \rightarrow Cl + NO_2} \tag{R7}$$

$$\mathrm{NO_2 + h\nu \rightarrow NO + O.} \tag{R8}$$

Figure 6 shows the formation and loss rates of NO to illustrate that these are the relevant reactions (the corresponding plots for $\mathrm{NO_2}$ look identical, but mirrored). The equilibrium condition derived from these reactions is

$$\frac{[\mathrm{NO}]}{[\mathrm{NO_2}]} = \frac{k_{R8}}{k_{R6}[\mathrm{O_3}] + k_{R7}[\mathrm{ClO}]}. \tag{3}$$

In the southern hemisphere during daytime, the fraction of NO compared to $\mathrm{NO_2}$ is much higher than in the northern hemisphere (80 %–90 % NO and 10 %–20% $\mathrm{NO_2}$ in the southern hemisphere, and 20 %–40 % NO and 60 %–80 % $\mathrm{NO_2}$ in the northern hemisphere, see Figure 5 and ~~percentage plots~~ Figures 7, 31, 55, 79 in the supplement). The relative partitioning is approximately constant between $70\,\mathrm{hPa}$ and $32\,\mathrm{hPa}$ (~~see~~ Figures 7, 31, 55, 79 of the supplement). The higher NO levels are caused by the much lower ozone levels in the southern hemisphere (see Figure 19), which ~~shifts~~ shift the equilibrium by hindering the $\mathrm{O_3 + NO}$ reaction (e.g. Douglass et al., 1995). At night, no NO is present, since the reaction $\mathrm{NO_2 + h\nu}$ does not take place. $\mathrm{NO_3}$ does not significantly contribute to the budget of $\mathrm{NO_x}$ due to the fast reaction into $\mathrm{NO_2}$ by

$$\mathrm{NO_3 + h\nu \rightarrow NO_2 + O} \tag{R9}$$

during daytime and into $\mathrm{N_2O_5}$ at night (see discussion of R13).

Despite the relatively low mixing ratios, $\mathrm{NO_x}$ plays an important role in the chemistry of polar ozone depletion (the ~~gas phase~~ gas-phase catalytic $\mathrm{NO_x}$ cycle is in general an important contributor to stratospheric ozone chemistry, e.g. outside of the vortex and in higher altitudes than discussed here). In addition to the equilibrium between NO and $\mathrm{NO_2}$, there is a fast equilibrium between $\mathrm{NO_2}$ and $\mathrm{ClONO_2}$ under sunlit conditions, so that all three species are coupled. $\mathrm{ClONO_2}$ is to a good approximation in an equilibrium between

$$
\begin{aligned}
\mathrm{ClONO_2 + h\nu} &\rightarrow \mathrm{Cl + NO_3} \tag{R10}\\
&\rightarrow \mathrm{ClO + NO_2} \tag{R11}
\end{aligned}
$$

and

$$\mathrm{ClO + NO_2 + M \rightarrow ClONO_2 + M} \tag{R12}$$

see e.g. Portmann et al. (1996). Reaction R10 is the dominant branch of the $\mathrm{ClONO_2}$ photolysis. The equilibrium condition for $\mathrm{ClONO_2}$ can be written as

$$[\mathrm{ClO}][\mathrm{NO_2}] = \frac{k_{R10} + k_{R11}}{k_{R12}}[\mathrm{ClONO_2}]. \tag{4}$$
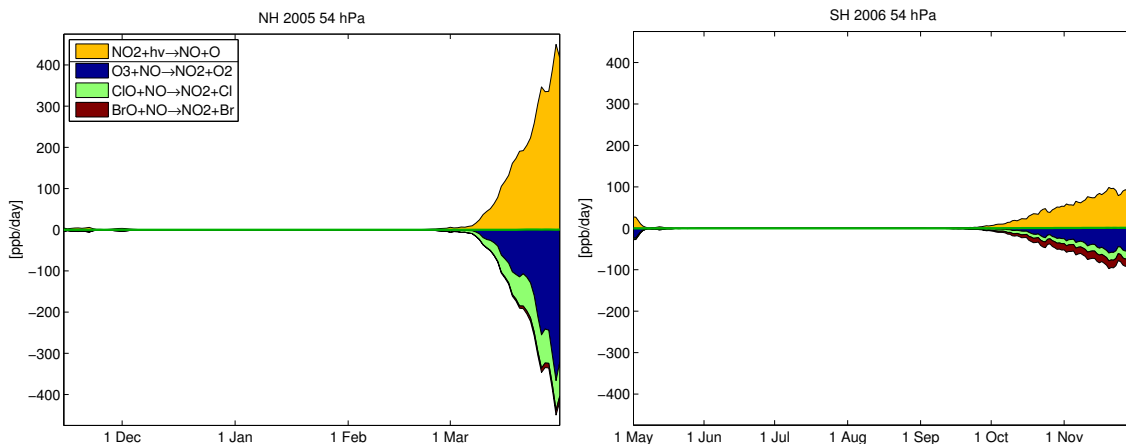
Figure 6. Vortex-averaged chemical reaction rates of reactions changing NO for the Arctic winter 2004/2005 (left) and the Antarctic winter 2006 (right) at 54 hPa to illustrate NO_x partitioning. Production reactions are shown positive and are separated by a line in the legend from the loss reactions, which are shown negative. The net change of NO is shown as a green line.

Alternatively, since NO and NO_2 are in equilibrium, this can also be expressed in terms of NO

$$[ClO][NO] = \frac{(k_{R10} + k_{R11})k_{R8}[ClONO_2]}{k_{R12}(k_{R6}[O_3] + k_{R7}[ClO])}. \tag{5}$$
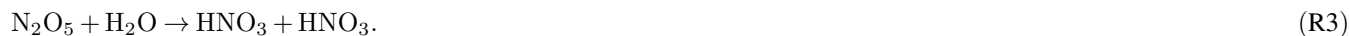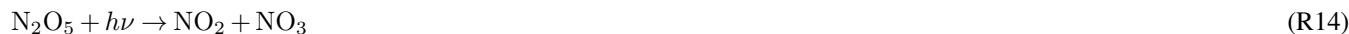
Production of NO_x from HNO_3 in spring will increase NO_2. In turn, $ClONO_2$ will increase almost instantly at the expense of NO_2 to match the equilibrium condition again. In this sense, $ClONO_2$ is produced from HNO_3 via NO_x in spring (e.g.
5 Portmann et al., 1996). This is an important deactivation pathway for active chlorine in the northern hemisphere, since it consumes ClO.

There is a striking difference in $ClONO_2$ production in spring between the northern and southern hemisphere (Figure 5). While $ClONO_2$ increases to 2 ppb in the northern hemisphere, it stays below 0.1 ppb in the southern hemisphere due to the strongly denitrified conditions there. The hindrance of the deactivation path via $ClONO_2$ under denitrified conditions prolongs
10 the period of ozone loss, since the other deactivation path via the reaction $Cl + CH_4$ is only effective under low ozone levels (e.g. Douglass et al., 1995, Portmann et al., 1996), see Section 4.3.2. $ClONO_2$ stays relatively constant in March 2005 in the northern hemisphere after the initial increase, since the decrease in ClO is compensated by an increase in NO_2.
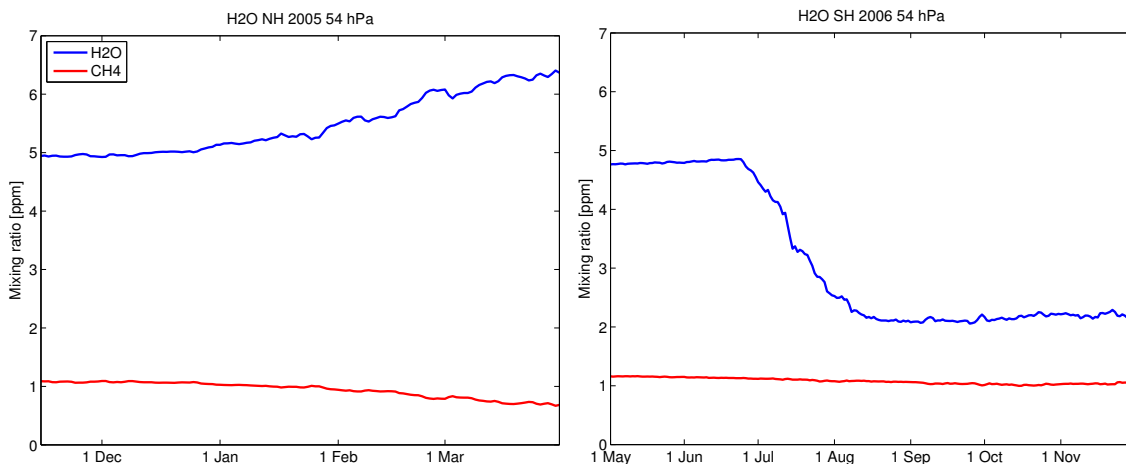
The mixing ratio of N_2O_5 is governed by

$$NO_2 + NO_3 + M \rightarrow N_2O_5 + M \tag{R13}$$

15

$$N_2O_5 + h\nu \rightarrow NO_2 + NO_3 \tag{R14}$$

$$N_2O_5 + H_2O \rightarrow HNO_3 + HNO_3. \tag{R3}$$

13

Figure 7. Vortex-averaged mixing ratios of H_2O and CH_4 for the Arctic winter 2004/2005 and the Antarctic winter 2006 at $54\,hPa$.

At night N_2O_5 is produced slowly by reaction R13, with NO_3 produced by

$$NO_2 + O_3 \rightarrow NO_3 + O_2. \tag{R15}$$

During daytime, no N_2O_5 is produced, since the NO_3 produced by reactions R10 and R15 is easily photolyzed. However, N_2O_5 is only slowly depleted during daytime, so that N_2O_5 levels during daytime and at night are comparable in the northern hemisphere (up to $30\,\%$ of classical NO_x is in N_2O_5). In the southern hemisphere, low ozone levels hinder the production of N_2O_5. The produced N_2O_5 can react back to the reservoir HNO_3 via reaction R3 (see Figure 4).

4.2 Hydrogen species

The sources for $HO_x = OH + HO_2$ are mainly H_2O, CH_4 and HNO_3. The source for stratospheric water is humid tropospheric air "freeze-dried" at the tropopause and sources for CH_4 are both natural (e.g. wetlands) and anthropogenic (e.g. WMO, 2011; Montzka, 2012). CH_4 is slowly oxidized to H_2O in the stratosphere (e.g. Hanisco, 2003, see also below). Figure 7 shows that the mixing ratio for H_2O is between $2\,ppm$ and $6\,ppm$ at $54\,hPa$ and that CH_4 has a mixing ratio of about $1\,ppm$. The decrease of H_2O in July 2006 in the southern hemisphere is caused by dehydration by sedimenting cloud particles, similar to the situation for HNO_3. The northern hemisphere in 2005 is not cold enough for the formation of a significant amount of ice clouds (Figure 1).

Production and loss processes of HO_x are fairly complicated (Hanisco, 2003). Figure 8 shows the production and loss rates of an extended HO_x at $54\,hPa$, where we have included some species that are not a net source or sink of HO_x over a diurnal cycle (extended $HO_x = OH + HO_2 + H + HOCl + HOBr + HO_2NO_2$). Particularly in the southern hemisphere, ~~production~~ CH_4 oxidation plays an important role. Production from CH_4 oxidation ~~, which~~ can be initiated by
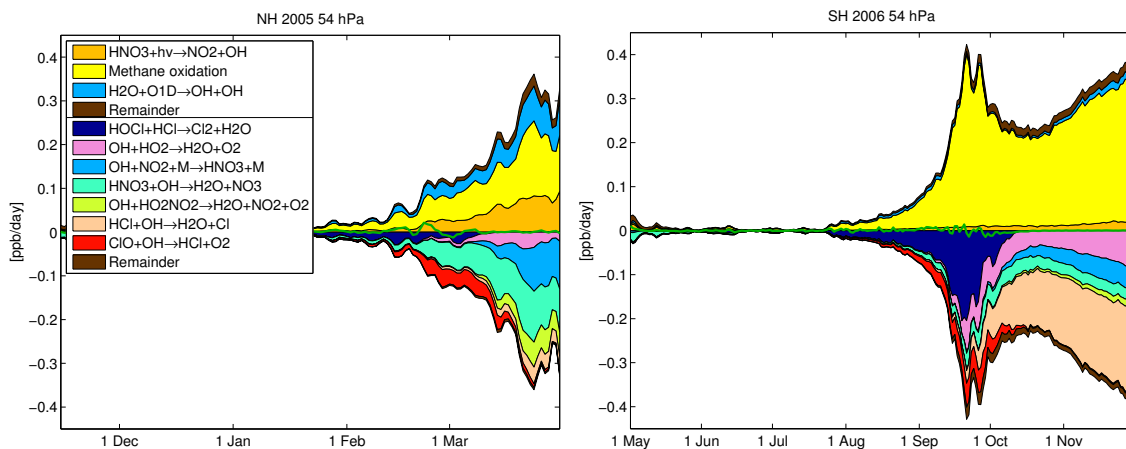
$$X + CH_4 \rightarrow XH + CH_3 \tag{R16}$$

14

Figure 8. Vortex-averaged chemical reaction rates of reactions changing extended HO_x ($OH + HO_2 + H + HOCl + HOBr + HO_2NO_2$) for the Arctic winter 2004/2005 (left) and the Antarctic winter 2006 (right) at 54 hPa. Production reactions are shown positive and are separated by a line in the legend from the loss reactions, which are shown negative. The net change of extended HO_x is shown as a green line. Methane oxidation is modelled by simplified net reactions in ATLAS, the reactions denoted as methane oxidation in the legend are $Cl + CH_4 \rightarrow HCl + CH_2O + HO_2$ and $Cl + CH_2O \rightarrow HCl + CO + HO_2$.

with ~~X = Cl, O(^{1}D), OH plays an important role. It~~ $\underline{X = Cl, O(^1D)\ or}$ OH $\underline{and}$ then continues with a complicated chain of reactions involving CH_2O (see Hanisco, 2003, for more details). The maximum yield of this reaction chain is 4 HO_x per CH_4, but the yield is normally lower (Hanisco, 2003). For example, the HCl formed by R16 with $X = Cl$ lowers the yield of the reaction chain starting with this reaction because of the reaction

5
$$HCl + OH \rightarrow H_2O + Cl. \tag{R17}$$

Reaction of water with $O(^1D)$

$$H_2O + O(^1D) \rightarrow OH + OH \tag{R18}$$

and photolysis of HNO_3

$$HNO_3 + h\nu \rightarrow NO_2 + OH \tag{R1}$$

10 can also produce HO_x. Sinks are the recombination into water

$$OH + HO_2 \rightarrow H_2O + O_2 \tag{R19}$$

and the reactions

$$OH + NO_2 + M \rightarrow HNO_3 + M \tag{R5}$$

15

$$HNO_3 + OH \rightarrow H_2O + NO_3 \tag{R2}$$

$$ClO + OH \rightarrow HCl + O_2. \tag{R20}$$

5 HO_x is in equilibrium with HOCl under sunlit conditions and when chlorine is activated (e.g. Portmann et al., 1996)

$$HOCl + h\nu \rightarrow Cl + OH \tag{R21}$$

$$ClO + HO_2 \rightarrow HOCl + O_2. \tag{R22}$$

Hence, the heterogeneous reaction

10 $$HOCl + HCl \rightarrow Cl_2 + H_2O \tag{R23}$$

is also a sink for HO_x. The rates of the reactions changing extended HO_x increase by up to a factor of 4 from $70\,hPa$ to $32\,hPa$ (see Figures 10, 34, 58, 82 of the supplement). The relative importance of the reactions does not change with the exception of methane oxidation, which becomes less important with increasing height.

HO_x levels are about 1 to $4\,ppt$ at $54\,hPa$ under sunlit conditions in both hemispheres (Figure 9). Maximum values typically

15 increase from $3\,ppt$ at $70\,hPa$ to $7\,ppt$ at $32\,hPa$ (Figures 11, 35, 59, 82 in the supplement). At night, no HO_x is present, since there is no production and HO_x recombines into water and HNO_3 (Figure 8). HOCl can reach mixing ratios of up to $0.15\,ppb$ at $54\,hPa$ in both hemispheres, as long as chlorine is activated (see Figure 11). Figure 9 shows that HO_x does not simply scale with the amount of sunlight, HNO_3, H_2O and CH_4: In the southern hemisphere, HO_x shows a peak under conditions of both chlorine activation and sunlight, related to the fact that reactions like $Cl + CH_4$ and $HOCl + HCl$ play a role in HO_x chemistry

20 (Figure 8, see also the discussion in Section 4.3.2 related to HCl).

Figure 9 also shows the partitioning of HO_x. Similar to NO_x, there is a fast equilibrium between OH and HO_2. The partitioning between the HO_x species is determined mainly by
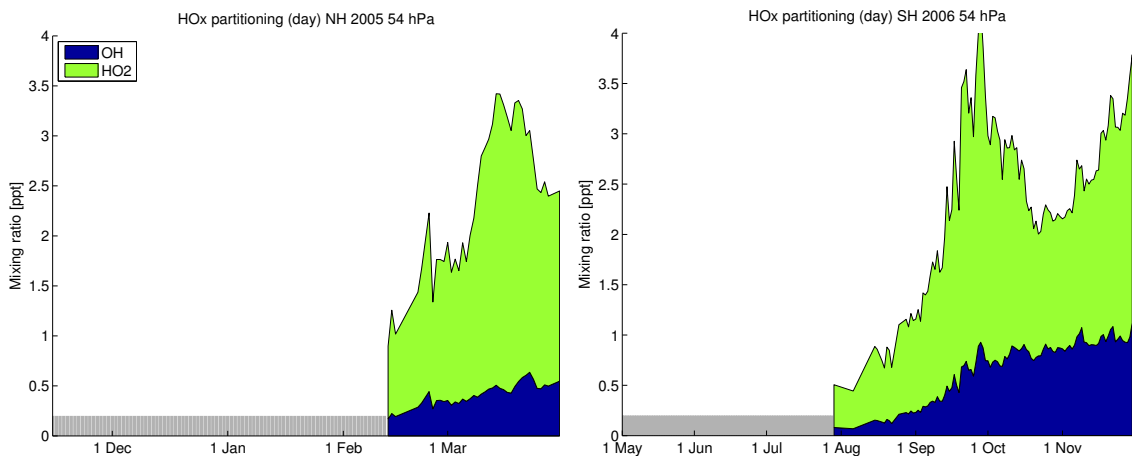
$$HOCl + h\nu \rightarrow Cl + OH \tag{R21}$$

25 $$ClO + HO_2 \rightarrow HOCl + O_2 \tag{R22}$$

$$ClO + OH \rightarrow Cl + HO_2 \tag{R24}$$

$$O_3 + HO_2 \rightarrow OH + 2\,O_2 \tag{R25}$$

Figure 9. Vortex-averaged partitioning of HO_x species for the Arctic winter 2004/2005 (left) and the Antarctic winter 2006 (right) at $54\,\mathrm{hPa}$. Daytime averages (parts of the vortex where the solar zenith angle is smaller than $80°$). Nighttime averages are near zero and not shown. Days without sufficient data for averaging are not shown (grey bars).

$$O_3 + OH \rightarrow HO_2 + O_2 \tag{R26}$$

$$NO + HO_2 \rightarrow NO_2 + OH. \tag{R27}$$

Figure 10 shows the rates of HO_2 production and loss (the corresponding plots for OH look similar, but mirrored, with $ClO + HO_2$ replaced by $HOCl + h\nu$).

The rates of the reactions partitioning HO_x increase by up to a factor of 4 from $70\,\mathrm{hPa}$ to $32\,\mathrm{hPa}$ ~~again (see~~ (Figures 13, 37, 61, 85 of the supplement), but the relative importance of the reactions does not change except for the reaction R24 getting less important with increasing altitude.

The production and loss rates of HO_x proper are dominated by the reactions R21 and R22 which form the equilibrium with HOCl (not shown).

The equilibrium is mainly on the side of HO_2 in both hemispheres (see Figure 9, e.g. Hanisco, 2003). The fraction of OH is somewhat higher in the southern hemisphere (about $20\,\%$–$40\,\%$) than in the northern hemisphere (about $10\,\%$–$20\,\%$), see also ~~percentage plots~~ Figures 12, 36, 60, 84 in the supplement. The relative partitioning is approximately constant with altitude (see supplement). Absolute OH levels are of relatively similar magnitude in both hemispheres (up to $1\,\mathrm{ppt}$ in the southern hemisphere and up to $0.5\,\mathrm{ppt}$ in the northern hemisphere).

Equations for the equilibrium values of OH, HO_2 and HOCl can be derived from reactions R21 to R27. The ratio of OH and HO_2 under sunlit conditions in the northern hemisphere and in the southern hemisphere before mid-September is to a good
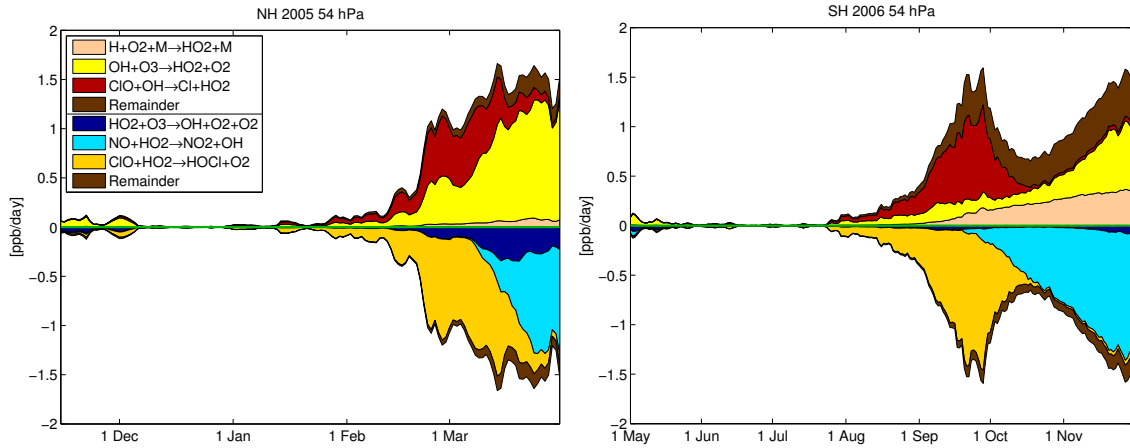
17

Figure 10. Vortex-averaged chemical reaction rates of reactions changing HO_2 for the Arctic winter 2004/2005 (left) and the Antarctic winter 2006 (right) at 54 hPa to illustrate HO_x partitioning. Production reactions are shown positive and are separated by a line in the legend from the loss reactions, which are shown negative. The net change of HO_2 is shown as a green line.

approximation given by

$$\frac{[\mathrm{OH}]}{[\mathrm{HO_2}]} = \frac{k_{R25}[\mathrm{O_3}] + k_{R22}[\mathrm{ClO}] + k_{R27}[\mathrm{NO}]}{k_{R26}[\mathrm{O_3}] + k_{R24}[\mathrm{ClO}]}. \tag{6}$$

That is, the ratio depends only on O_3, ClO and NO. The equation can be simplified to

$$\frac{[\mathrm{OH}]}{[\mathrm{HO_2}]} = \frac{k_{R25}[\mathrm{O_3}] + k_{R22}[\mathrm{ClO}]}{k_{R26}[\mathrm{O_3}] + k_{R24}[\mathrm{ClO}]} \tag{7}$$

5 under conditions when chlorine is activated and no NO is present (see Figure 5, before March 2005 and mid-September 2006 in the northern and southern hemisphere, respectively) and to

$$\frac{[\mathrm{OH}]}{[\mathrm{HO_2}]} = \frac{k_{R25}[\mathrm{O_3}] + k_{R27}[\mathrm{NO}]}{k_{R26}[\mathrm{O_3}]} \tag{8}$$

in spring in the northern hemisphere (end of March 2005), after chlorine is deactivated). In the southern hemisphere, the change between conditions rich in ClO_x and rich in NO_x is marked by a change in the relative ~~partitioning~~ contribution of OH to HO_x

10 from about 20 % to about 40 % at the start of October (see ~~percentage plots~~ Figures 60, 84 in the supplement). A similar discussion and expressions for mid-latitudes can be found in Cohen et al. (1994).

Under sunlit conditions and when chlorine is activated, the equilibrium of HOCl is given by

$$[\mathrm{HOCl}] = \frac{k_{R22}}{k_{R21}}[\mathrm{ClO}][\mathrm{HO_2}]. \tag{9}$$

At night, HOCl remains constant (except for heterogeneous processing), since neither the photolysis reaction nor the ClO +

15 HO_2 reaction can proceed.

18

HO_x is relevant for ozone depletion, since the reactions $HCl + OH \rightarrow H_2O + Cl$ (R17) and $ClO + OH \rightarrow HCl + O_2$ (R20) play a role in chlorine activation and deactivation (note that the second reaction differs from reaction R24 in the products). In addition, chlorine can be activated by the heterogeneous $HOCl + HCl$ (R23) reaction.

4.3 Chlorine species

4.3.1 Overview and partitioning

When the polar vortex forms, the majority of chlorine is present in the form of HCl and the remainder is present in the other important reservoir gas $ClONO_2$ (e.g. Solomon, 1999; Santee et al., 2008). Figure 11 shows the partitioning between the various inorganic chlorine species (Cl_y). The available amount of Cl_y is about 2.7 to 3.3 ppb at 54 hPa. The increase of Cl_y over the winter is due to transport from above. Due to ~~the~~ stronger descent in the model in the northern hemisphere, Cl_y increases to values that are about 0.3 ppb higher in the northern hemisphere in 2005 than in the southern hemisphere in spring 2006, although the initial values are similar. ~~This increases~~ Thus, the chlorine potentially available for ozone depletion in the northern hemisphere is increased compared to the southern hemisphere. In both hemispheres, the initial mixing ratio of HCl is about 2 ppb at 54 hPa (75 % of Cl_y) and the initial mixing ratio of $ClONO_2$ is about 0.7 ppb (see also Santee et al., 2008). Cl_y is produced by photolysis and reaction with $O(^1D)$ from chlorofluorocarbons (CFCs), hydrochlorofluorocarbons (HCFCs) and similar species of mainly anthropogenic origin (e.g. WMO, 2011; Montzka, 2012). The relative partitioning ~~inside~~ within Cl_y is approximately constant between 70 hPa and 32 hPa (with only a slight increase in Cl_y with altitude, see Figures 14, 38, 62, 86 of the supplement), so that most of the following discussion applies to the entire altitude range.

In early winter, passive reservoir gases HCl and $ClONO_2$ are transformed to Cl_2 through heterogeneous reactions on the surface of polar stratospheric clouds (e.g. Solomon et al., 1986), starting in December 2004 in the northern hemisphere and in May 2006 in the southern hemisphere. Since the major reaction that transforms the reservoir gases to Cl_2 is $HCl + ClONO_2$ (e.g. Solomon et al., 1986, see also Section 4.3.2), the amount of chlorine that can be activated is limited by the mixing ratio of the less abundant $ClONO_2$ (e.g. Portmann et al., 1996). While some $ClONO_2$ can be regenerated by the reaction $ClO + NO_2 + M$ and some HCl can be activated by the reaction $HOCl + HCl$, this is not sufficient to remove all HCl over the course of the winter, and total HCl mixing ratios consistently stay larger than 0.5 ppb in our model runs, while $ClONO_2$ decreases to near zero values. Due to the applied ~~correction~~ adjustment to the HCl solubility (see Section 6), up to 0.5 ppb of HCl is dissolved in STS droplets in the southern hemisphere at 54 hPa (more with increasing altitude).

When sunlight starts to come back, Cl_2 is quickly transformed to the active chlorine species ClO and its dimer Cl_2O_2 by photolysis of Cl_2

$$Cl_2 + h\nu \rightarrow Cl + Cl \tag{R28}$$

immediately followed by the reaction

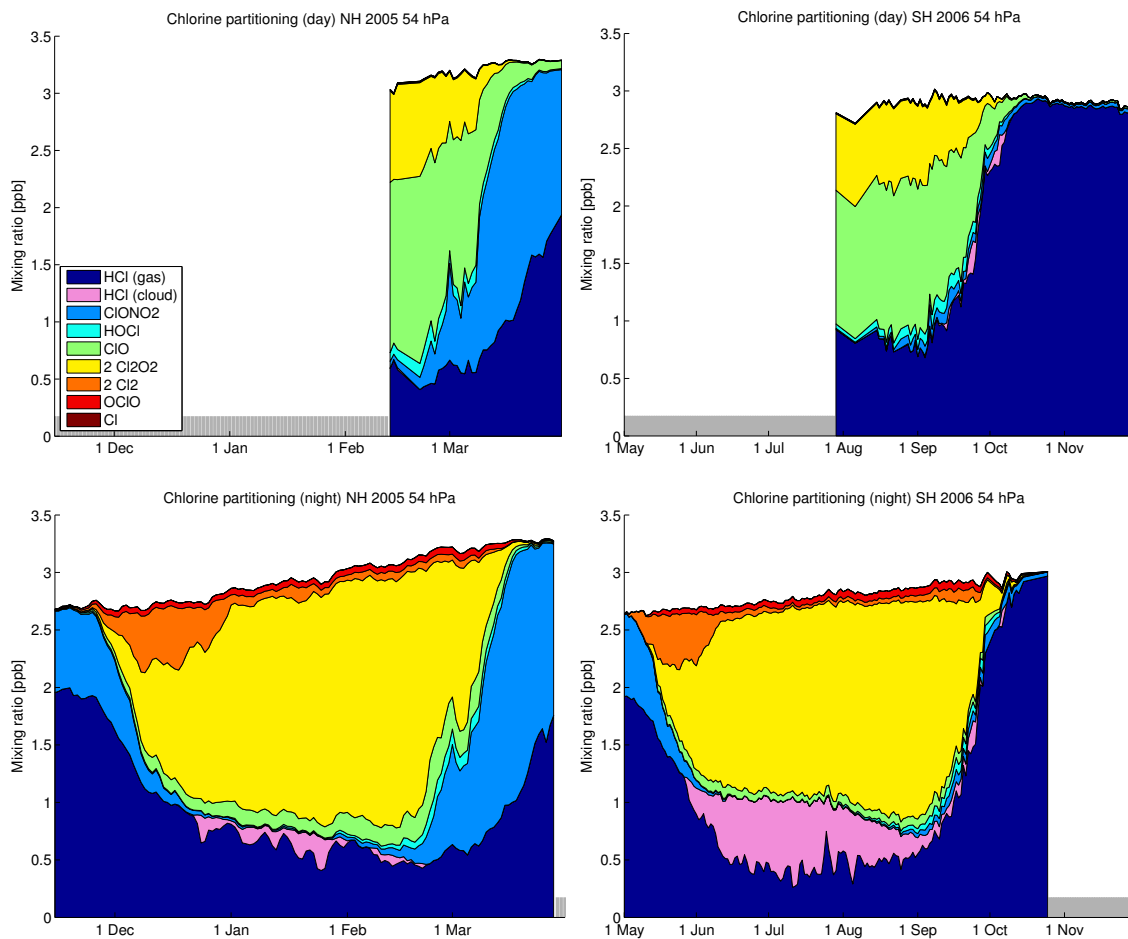$$Cl + O_3 \rightarrow ClO + O_2 \tag{R29}$$

19

Figure 11. Vortex-averaged partitioning of inorganic chlorine species (Cl_y) for the Arctic winter 2004/2005 (left) and the Antarctic winter 2006 (right) at 54 hPa. Top row: Daytime averages (parts of the vortex where the solar zenith angle is smaller than $80°$). Bottom row: Nighttime averages (parts of the vortex where the solar zenith angle is larger than $100°$). Days without sufficient data for averaging are not shown (grey bars). Species $ClNO_2$ and BrCl are not shown due to their small mixing ratios. The area labeled "HCl (cloud)" shows HCl dissolved in STS droplets due to the applied ~~correction~~ adjustment to the HCl solubility (see section 6).

to produce ClO. The time between first activation and the first sunlight becomes apparent in a Cl_2 peak in December 2004 and May 2006 in Figure 11.

Under polar conditions, the dimer of ClO plays an important role. Reactions that determine the ratio of ClO and its dimer Cl_2O_2 are

5
$$ClO + ClO + M \rightarrow Cl_2O_2 + M \tag{R30}$$

$$Cl_2O_2 + h\nu + M \rightarrow 2\,Cl + O_2 + M \tag{R31}$$

$$Cl_2O_2 + M \rightarrow ClO + ClO + M. \tag{R32}$$

10 Reactions R30 and R31 are part of the ClO dimer ozone loss cycle and play an important role in ozone depletion (see Section 4.5). Note that reaction R31 includes an intermediate step over ClOO not shown here. Figure 12 shows the partitioning of $ClO_x = ClO + 2\,Cl_2O_2$ at 54 hPa. Active chlorine is mainly present in the form of Cl_2O_2 at night and in the form of ClO during daytime (e.g. Stimpfle et al., 2004; WMO, 2011). At night, only small levels of ClO (10 % of ClO_x in our model) are maintained by the interplay between the forward reaction R32 (thermal dissociation) and backward reaction R30 (e.g. Stimpfle
15 et al., 2004; WMO, 2011). The nighttime equilibrium is highly temperature dependent (e.g. Stimpfle et al., 2004), and higher temperatures shift the equilibrium towards ClO at night (see Figure 12). During daytime, most Cl_2O_2 is photolyzed into Cl, which reacts to ClO~~and there is an~~, and equilibrium between ClO and Cl_2O_2 ~~by~~ is maintained through the photolysis reaction R31 and reaction R30 (e.g. WMO, 2011). About 70 % of ClO_x is present as ClO during daytime ~~in~~ at all altitudes in our model (Figure 12 and Figures 16, 40, 64, 88 of the supplement). This is in good agreement with the 60 %–70 % inferred from direct
20 aircraft observations of ClO and ClOOCl by Stimpfle et al. (2004). ~~Modelled ClO values are also in reasonable agreement with MLS measurements in the northern hemisphere in 2005 and in the southern hemisphere in 2006 (see supplement).~~

There is a long history of studies investigating the reactions R30 to R32, which are central for polar ozone depletion and have been uncertain for a long time (e.g. Molina and Molina, 1987; Burkholder et al., 1990; Stimpfle et al., 2004; Frieler et al., 2006; Schofield et al., 2008; Kremser et al., 2011; Canty et al., 2016). Recently, a study of the photolysis cross section of
25 Cl_2O_2 challenged the understanding of polar ozone depletion and ~~caused~~ motivated a thorough reinvestigation of the chemistry of ozone depletion (see WMO, 2011, section 2.2.2 and references therein). The uncertainties have been resolved (Kawa et al., 2009; WMO, 2011; von Hobe and Stroh, 2012; Canty et al., 2016), but the Cl_2O_2 photolysis is still one of the reactions that causes the largest uncertainties in ozone depletion (Kawa et al., 2009). In addition, there is ~~also~~ some uncertainty in the nighttime equilibrium between ClO and Cl_2O_2 (Kawa et al., 2009; Canty et al., 2016), but this is not relevant for the amount
30 of ozone depletion.

When chlorine is activated (from December 2004 to the beginning of March 2005 in the northern hemisphere and from May ~~2006 to September~~ to the beginning of October 2006 in the southern hemisphere), ozone is removed by the ClO dimer cycle

and the ClO–BrO cycle (e.g. Solomon, 1999, see also Section 4.5). ClO_x peaks at about 2.4 ppb in the northern hemisphere and at about 2.0 ppb in the southern hemisphere at 54 hPa, with little variation from 70 hPa to 32 hPa (see Figures 15, 39, 63, 87 of the supplement).

Modelled ClO values are in reasonable agreement with MLS measurements in the northern hemisphere in 2005, but are underestimated by 0.2–0.4 ppb in the southern hemisphere in 2006 (Figures 145, 147, ..., 163 of the supplement). In the measurements, the highest peak values of ClO are typically about 2.0 ppb in both hemispheres, but in the model in the southern hemisphere, only 1.6-1.8 ppb are reached. This is consistent with an overestimation of gas-phase HCl compared to MLS of the same order of magnitude (see Section 6), which means that the discrepancy in ClO is directly related to the difficulty to model HCl correctly.

~~The~~ In the model, the higher peak values of ClO_x in the northern hemisphere are caused not only by the higher Cl_y values (Figure 11), but also by the more efficient activation of HCl into ClO_x by reformation of $ClONO_2$ in the northern hemisphere, which provides about 0.1–0.2 ppb additional chlorine from HCl compared to the southern hemisphere (see discussion in the section "HCl loss" below). However, the underestimation of ClO and overestimation of HCl by ATLAS compared to MLS in the southern hemisphere point at an underestimation of chlorine activation in the southern hemisphere. Taking this into account, similar ClO_x levels are expected in the real atmosphere in both hemispheres, and more efficient chlorine activation in the southern hemisphere compared to the northern hemisphere in the real atmosphere would be countered by higher Cl_y levels in the northern hemisphere to give similar ClO_x levels.

4.3.2   Reservoir HCl

Figure 13 shows the time evolution of the vortex-averaged reaction rates of all relevant reactions that change HCl at 54 hPa. The supplement shows that the rates and relative importance of the reactions are similar from 70 hPa to 32 hPa, so that the following discussion applies to the entire altitude range (Figures 17, 41, 65, 89 of the supplement). In early winter (up to the end of December 2004 in the northern hemisphere and up to the end of July 2006 in the southern hemisphere), HCl is removed by heterogeneous reactions on polar stratospheric clouds and active chlorine is produced. When sunlight returns, this is followed by a phase of competition between HCl removal by heterogeneous reactions and deactivation of ClO_x into HCl by gas-phase reactions (e.g. Portmann et al., 1996; Solomon et al., 2015), most pronounced in August 2006 in the southern hemisphere. In the southern hemisphere, this is followed by a phase of deactivation of active chlorine into HCl by the $Cl + CH_4$ reaction in September to October (e.g. Douglass et al., 1995). Finally, when sunlight comes back, the gas-phase loss reaction $HCl + OH$ becomes important and competes with the production by $Cl + CH_4$. In the southern hemisphere, HCl is near equilibrium during this time, while in the northern hemisphere, chlorine that was initially deactivated into $ClONO_2$ is slowly transformed into HCl.
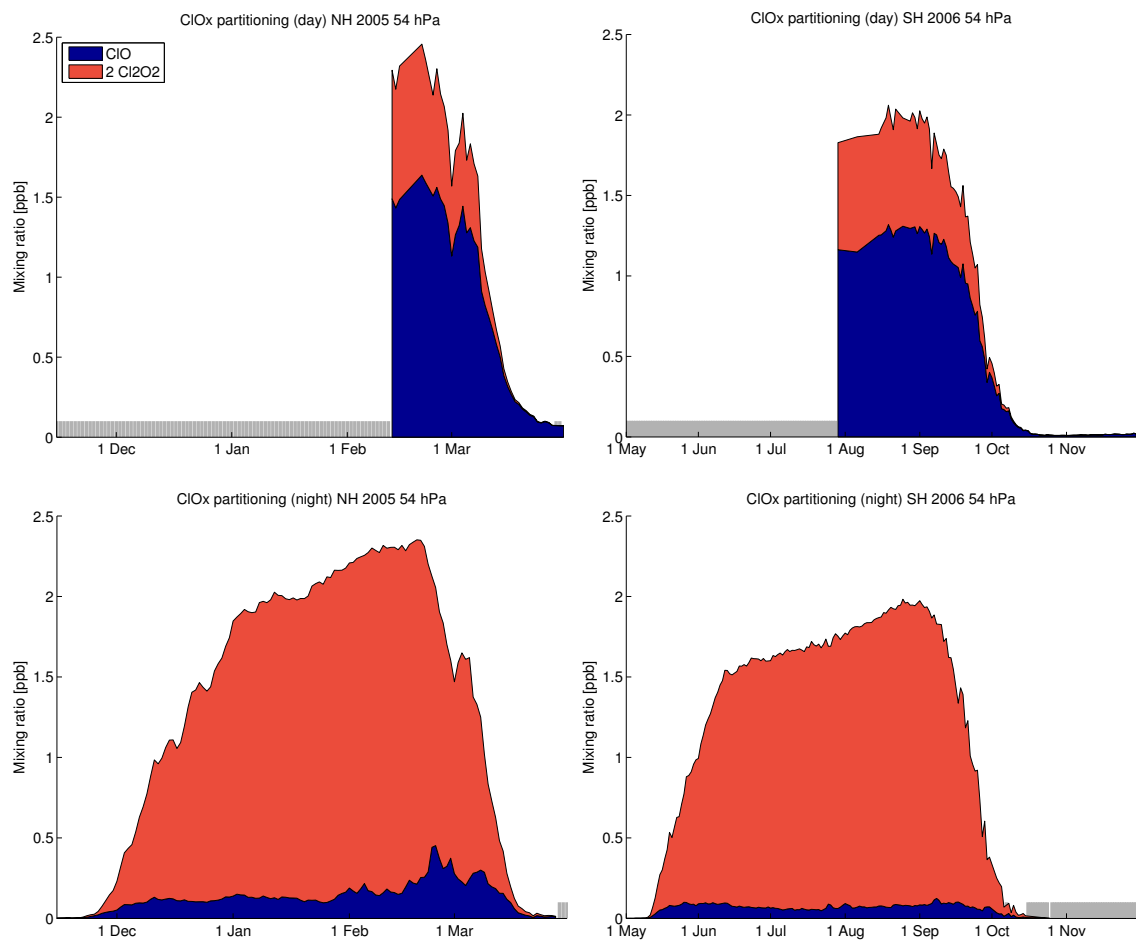
Figure 12. Vortex-averaged partitioning of ClO_x for the Arctic winter 2004/2005 (left) and the Antarctic winter 2006 (right) at $54\,hPa$. Top row: Daytime averages (parts of the vortex where the solar zenith angle is smaller than $80°$). Bottom row: Nighttime averages (parts of the vortex where the solar zenith angle is larger than $100°$). Days without sufficient data for averaging are not shown (grey bars).

23

HCl loss (chlorine activation)

The most important heterogeneous loss reaction for HCl is

$$ClONO_2 + HCl \rightarrow Cl_2 + HNO_3. \tag{R4}$$

Another heterogeneous activation channel for HCl is

5   $$HOCl + HCl \rightarrow Cl_2 + H_2O. \tag{R23}$$

While this reaction plays a smaller role in the northern hemisphere in 2005, the reaction is important in the southern hemisphere in the months August and September 2006. In the southern hemisphere, the $HOCl + HCl$ reaction accounts for about 70 % of the HCl activation by heterogeneous reactions (integrated over the winter) and in the northern hemisphere it accounts for about 30 %. HOCl only exists in significant amounts when chlorine is activated. In the southern hemisphere, there is a shift from

10 activation by $ClONO_2 + HCl$ in early winter to activation dominated by $HOCl + HCl$ later in spring. The reason for this is the deactivation of chlorine by the reaction $Cl + CH_4$ in the southern hemisphere (caused by the low ozone values, see next section below), which provides HCl and produces HO_x and in turn HOCl (for a detailed discussion, see Crutzen et al., 1992, Portmann et al., 1996). This can clearly be seen in the rising HCl levels in September in the southern hemisphere (Figure 11) and in the increased HO_x levels (Figure 9). In contrast, deactivation is mainly into $ClONO_2$ in the northern hemisphere, keeping HCl

15 levels low. Since the southern hemisphere is more denitrified, activation by $ClONO_2 + HCl$ is hindered. Note that the net effect of $Cl + CH_4$ and $HOCl + HCl$ is a net chlorine deactivation in the southern hemisphere (green line in Figure 13).

It is evident that ~~initially~~ about 0.1–0.2 ppb more HCl is removed in the northern hemisphere in December 2005 than in the southern hemisphere in May 2006 (Figure 11), although the temperatures are lower in the southern hemisphere and the initial values of HCl and $ClONO_2$ are similar. Figure 13 shows that the reason is that the $ClONO_2 + HCl$ reaction activates

20 more HCl in the northern hemisphere. This is caused by reformation of $ClONO_2$ after the initial depletion in the northern hemisphere (see Figure 17 below), which is much smaller in the southern hemisphere.

The only other reaction that removes HCl in relevant quantities is the gas-phase reaction with OH, which is only important under sunlit conditions:

$$HCl + OH \rightarrow H_2O + Cl. \tag{R17}$$

25 In the northern hemisphere, the reaction is relevant in March in 2005. For the southern hemisphere, the reaction is relevant in October 2006 and later.

HCl production (chlorine deactivation)

HCl is only produced by reactions that are indirectly dependent on sunlight. Deactivation of active chlorine occurs mainly into HCl in the southern hemisphere but predominantly into $ClONO_2$ in the northern hemisphere. The reason for this is that

30 deactivation into $ClONO_2$ is hindered in the southern hemisphere by strong denitrification (absence of NO_2), while normally it would be the preferred pathway of deactivation (e.g. Douglass et al., 1995; Portmann et al., 1996).
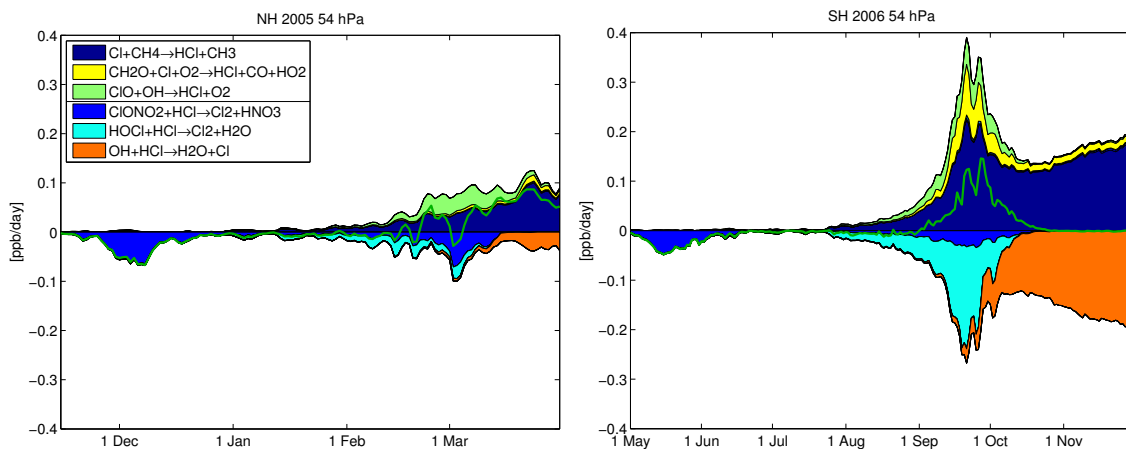
Figure 13. Vortex-averaged chemical reaction rates of reactions involving HCl for the Arctic winter 2004/2005 (left) and the Antarctic winter 2006 (right) at 54 hPa. Production reactions are shown positive and are separated by a line in the legend from the loss reactions, which are shown negative. The net change of HCl is shown as a green line. Reactions with rates which cannot be distinguished from the zero line at plot resolution are not shown.

In the long term, the partitioning of HCl and $ClONO_2$ in spring and summer favors HCl (e.g. Portmann et al., 1996; Santee et al., 2008). This can be seen in the fact that in the northern hemisphere, HCl is produced from $ClONO_2$ in spring after ClO_x has been deactivated into $ClONO_2$ some time earlier (see also Section 4.3.3 and Figure 17), while in the southern hemisphere, active chlorine is deactivated mainly into HCl. The chemical change rates of both HCl and $ClONO_2$ decrease to zero in

5 November in the southern hemisphere (green lines in Figures 13, 16 and 17). The reaction

$$Cl + CH_4 \rightarrow HCl + CH_3 \tag{R33}$$

is the main production reaction for HCl in both hemispheres (e.g. Portmann et al., 1996). In addition, it is responsible for deactivation under ozone hole conditions in the southern hemisphere. The reaction

$$ClO + OH \rightarrow HCl + O_2 \tag{R20}$$

10 becomes similar in importance to $Cl + CH_4$ as a production process for HCl around late February 2005 in the northern hemisphere, and plays a smaller role earlier and later in winter. In the southern hemisphere, the reaction is not negligible around September and October 2006. The reaction is responsible for part of the chlorine deactivation in both hemispheres. The reaction $ClO + OH$ has two product channels. The channel into HCl yields about 8 % of the products (the other channel is into Cl).
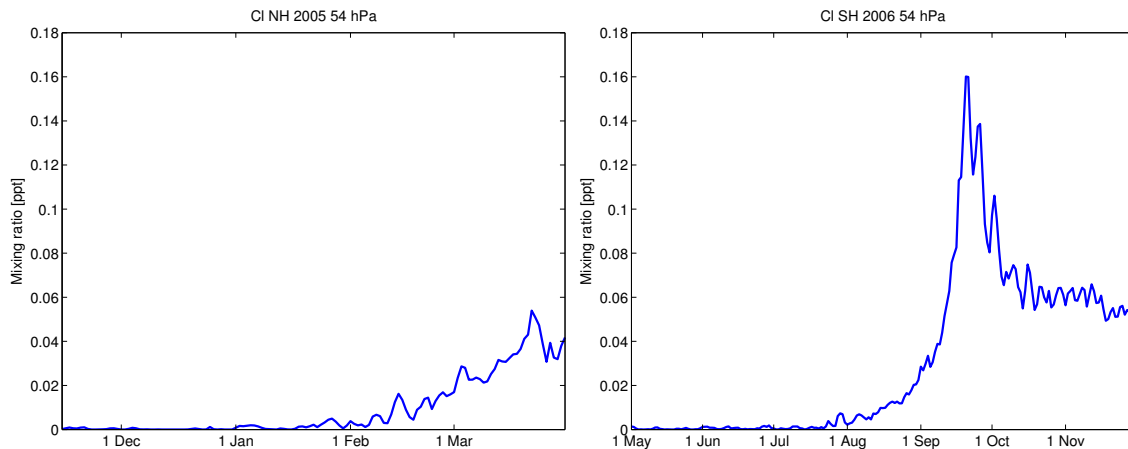
25

Figure 14. Vortex-averaged Cl mixing ratios for the Arctic winter 2004/2005 and the Antarctic winter 2006 at 54 hPa.

The role of Cl in HCl production

The rate of the $Cl + CH_4$ reaction is proportional to the mixing ratio of Cl. Figure 14 shows the mixing ratio of Cl for both hemispheres. Figure 15 shows that Cl is determined by the two source reactions

$$Cl_2O_2 + h\nu + M \rightarrow 2\,Cl + O_2 + M \tag{R31}$$

5

$$ClO + NO \rightarrow Cl + NO_2 \tag{R7}$$

and a reaction that removes Cl

$$Cl + O_3 \rightarrow ClO + O_2. \tag{R29}$$

Reaction R31 is coupled to the catalytic ClO dimer cycle. Cl levels are considerably higher in the southern hemisphere due
10 to a lack of ozone, which hinders the recombination to ClO (e.g. Douglass et al., 1995). This favors the deactivation of active chlorine via the $Cl + CH_4$ reaction (e.g. Portmann et al., 1996). Cl shows a very distinct behaviour in the southern hemisphere. It does not just increase with the amount of sunlight, but shows a peak in September, followed by a near constant plateau. This curve shape is approximately repeated in the curves of the reaction rate of the $Cl + CH_4$ reaction (Figure 13), since CH_4 is relatively constant. Figure 15 shows that the peak in Cl mixing ratios in the southern hemisphere is related to reaction R31, i.e.
15 the catalytic ozone destruction. In contrast, the plateau is related to the NO_x reaction R7 (see also Wayne et al., 1995, p. 2836).

4.3.3 Reservoir ClONO$_2$

Figure 16 shows the reaction rates of the most important reactions changing $ClONO_2$. The reaction rates increase by a factor of 2 from 70 hPa to 32 hPa in 2004/2005, but are more constant in 2009/2010 (~~see~~ Figures 20, 44 of the supplement). As
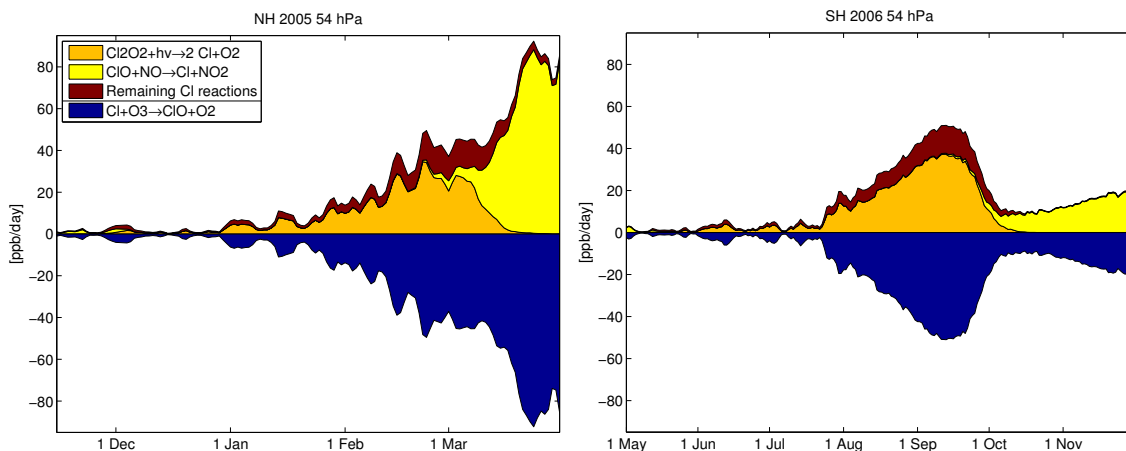
26

Figure 15. Vortex-averaged chemical reaction rates of reactions involving Cl for the Arctic winter 2004/2005 (left) and the Antarctic winter 2006 (right) at 54 hPa. Production reactions are shown positive and are separated by a line in the legend from the loss reactions, which are shown negative.

discussed in Section 4.1, the gross change rates of $ClONO_2$ are dominated by a near equilibrium between the reactions

$$ClONO_2 + h\nu \rightarrow Cl + NO_3 \tag{R10}$$

$$\rightarrow ClO + NO_2 \tag{R11}$$

5 and

$$ClO + NO_2 + M \rightarrow ClONO_2 + M \tag{R12}$$

under sunlit conditions (e.g. Portmann et al., 1996). Net changes of $ClONO_2$ are induced by changes in NO_x which shift the equilibrium (e.g. Portmann et al., 1996).

The net change of $ClONO_2$ is one order of magnitude smaller than the gross rates. Figure 17 shows the net effect of R10–R12
10 and all other reactions that play a role in changing $ClONO_2$. These reactions, which are all loss reactions, remove $ClONO_2$ either by heterogeneous reactions or gas-phase reactions of $ClONO_2$ with a radical. The most important heterogeneous reaction is the same as for HCl

$$ClONO_2 + HCl \rightarrow Cl_2 + HNO_3. \tag{R4}$$
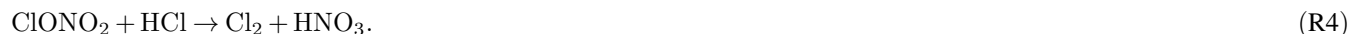
The reactions of $ClONO_2$ with a radical are of the type

15 $$ClONO_2 + X \rightarrow XCl + NO_3 \tag{R34}$$

where X is $X = O, Cl$ or OH. The reaction with Cl is the dominant reaction. The relative importance of these reactions is approximately constant from 70 hPa to 32 hPa (see Figures 21, 45, 69, 93 of the supplement).
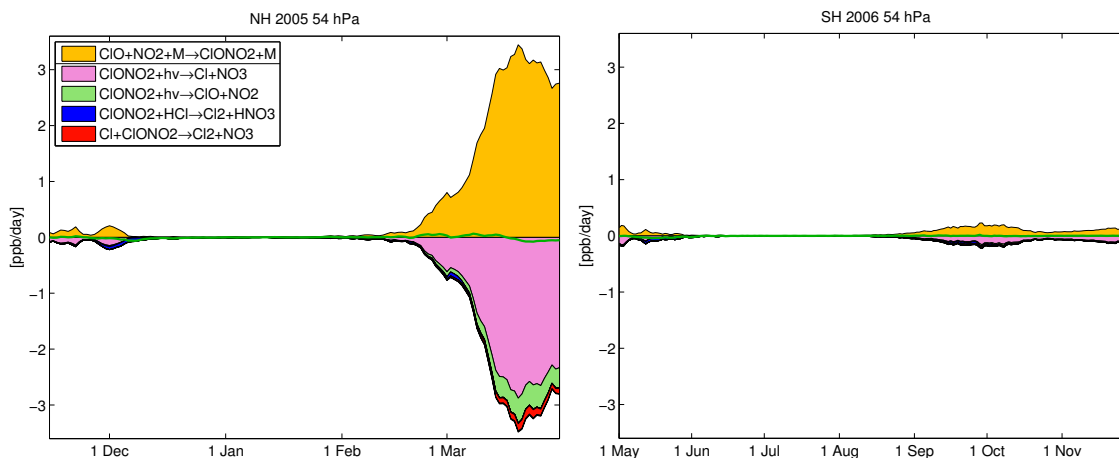
27

Figure 16. Vortex-averaged chemical reaction rates involving $ClONO_2$ for the Arctic winter 2004/2005 and the Antarctic winter 2006 at 54 hPa. Production reactions are shown positive and are separated by a line in the legend from the loss reactions, which are shown negative. The net change of $ClONO_2$ is shown as a green line. Reactions with rates which cannot be distinguished from the zero line at plot resolution are not shown.

In early winter in the polar night (December 2004 in the northern hemisphere, May and June 2006 in the southern hemisphere), the loss of $ClONO_2$ by heterogeneous reactions dominates, leading to the activation of chlorine. After the complete depletion of $ClONO_2$, this is followed by a phase with only small production and loss, due to near-zero levels of both NO_x and $ClONO_2$. The peak in production in early spring in the northern hemisphere (end of February and beginning of March 2005) is caused by the net production of extended NO_x from HNO_3 and is the main deactivation pathway for active chlorine in the northern hemisphere (e.g. Douglass et al., 1995; Portmann et al., 1996). At that time, $ClONO_2$ is out of equilibrium and more $ClONO_2$ is produced by $ClO + NO_2$ than is lost by photolysis. In the southern hemisphere, the rates are much lower due to the strongly denitrified conditions. In late March 2005, $ClONO_2$ is lost in the northern hemisphere and finally converted to HCl, which is the favored reservoir under summer conditions (e.g. Portmann et al., 1996; Santee et al., 2008). In the southern hemisphere, the rates of change are low in late October and November, since the deactivation already occurred directly into HCl.

4.4 Bromine species

Sources of inorganic bromine, which has both natural and anthropogenic sources, are mainly halons and methyl bromide, but also some short-lived species (e.g. WMO, 2011; Montzka, 2012). Inorganic bromine (Br_y) levels in the stratosphere are about 20 ppt at maximum (e.g. WMO, 2011), with marginally lower levels in the altitude range considered here. Bromine chemistry is still somewhat uncertain due to uncertainties in the reaction coefficients (Sander et al., 2011; von Hobe and Stroh, 2012).
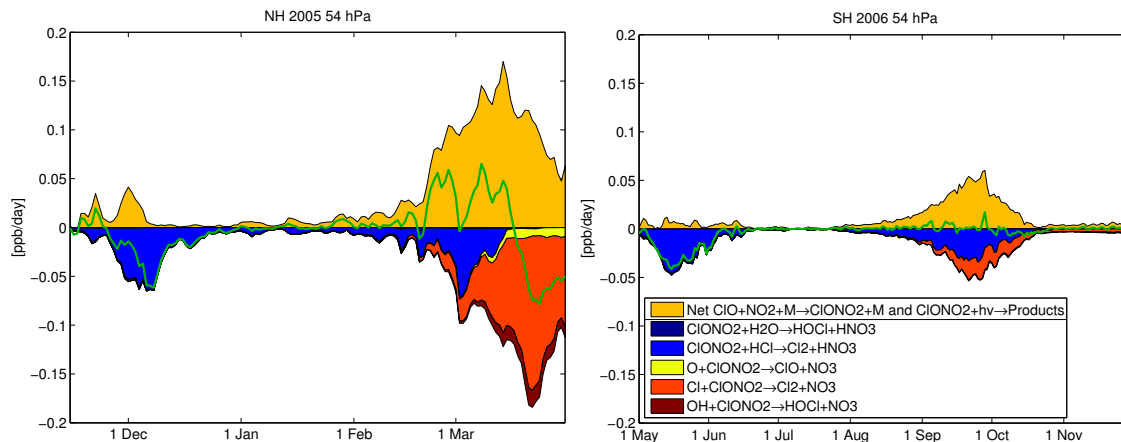
Figure 17. Vortex-averaged chemical reaction rates involving $ClONO_2$ for the Arctic winter 2004/2005 and the Antarctic winter 2006 at 54 hPa. In contrast to Figure 16, the net production rate of the fast cycle $ClONO_2 + h\nu \rightarrow Products \,/\, ClO + NO_2 + M \rightarrow ClONO_2 + M$ is shown. This cycle is separated by a line in the legend from the loss reactions. The green line shows the net change of $ClONO_2$ by chemistry. Reactions with rates which cannot be distinguished from the zero line at plot resolution are not shown.

Atomic bromine is released from the source gases mainly by photolysis. Under sunlit conditions, it is in equilibrium with BrO. The relevant reactions are

$$Br + O_3 \rightarrow BrO + O_2 \tag{R35}$$

5 $$BrO + h\nu \rightarrow Br + O \tag{R36}$$

$$BrO + NO \rightarrow NO_2 + Br \tag{R37}$$

$$BrO + ClO + M \rightarrow Br + Cl + O_2 + M. \tag{R38}$$

10 Reactions R35 and R38 are directly involved in the ClO–BrO cycle, see Section 4.5.

Figure 18 shows the partitioning between the various inorganic bromine species at 54 hPa, which is very similar from 70 hPa to 32 hPa (see Figures 22, 46, 70, 94 of the supplement). Bromine is mostly present in the form of HOBr and $BrONO_2$ at night before chlorine activation starts. In contrast to the less reactive chlorine, these are not real reservoir gases, since they easily photolyze into Br and react further to BrO during daytime, which gives bromine a great potential to destroy ozone despite

15 the low mixing ratios (e.g. Lary, 1996; Solomon, 1999). BrO is a dominant species during daytime (e.g. Lary, 1996), except

29

in October and November in the southern hemisphere, when the reaction $Br + O_3$ is hindered by the low ozone levels and Br mixing ratios are significant. Heterogeneous reactions play only a minor role and are not needed for activation (e.g. Lary et al., 1996; Wayne et al., 1995). As long as chlorine is activated, almost all bromine is in the form of BrCl at night (e.g. Lary et al., 1996; von Hobe and Stroh, 2012). BrCl is produced by the reaction

$$BrO + ClO \rightarrow BrCl + O_2. \tag{R39}$$

During daytime, most of this BrCl is transformed to Br by photolysis

$$BrCl + h\nu \rightarrow Br + Cl \tag{R40}$$

followed by transformation to BrO by reaction R35.

4.5 Oxygen species

Figure 19 shows the vortex-averaged mixing ratios of ozone for the northern and southern hemisphere. Ozone stays more constant in the northern hemisphere 2005 ~~compared to the southern hemisphere 2006 ((~~(where values range from 1.5 ppm to 2.5 ppm at 54 hPa) compared to the southern hemisphere 2006, since the change by ozone depletion is nearly cancelled by transport of air rich in ozone from above and over the vortex edge. In contrast, ozone values decrease from 2.5 ppm to less than 0.5 ppm at 54 hPa in the southern hemisphere in 2006, both due to weaker transport and larger ozone depletion. While the initial ozone value of 2.5 ppm in the northern hemisphere in 2004/2005 is relatively constant with height, the value at the end of the winter varies from 1 ppm at 70 hPa to 3 ppm at 32 hPa due to changes in ozone depletion, production and transport (~~see~~ Figure 23 of the supplement). In the warmer winter 2009/2010, values are more similar at the end of the winter and less ozone depletion is observed (~~see~~ Figure 47 of the supplement).

O_3 is in ~~a~~ very fast equilibrium with O. The dominant cycle is part of the well-known Chapman chemistry (Chapman, 1930)

$$O_3 + h\nu \rightarrow O + O_2 \tag{R41}$$

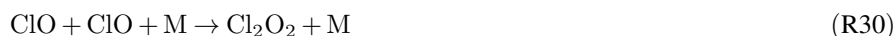$$O + O_2 + M \rightarrow O_3 + M. \tag{R42}$$

We follow the usual convention here to treat O_3 and O together as odd oxygen O_x (e.g. Brasseur and Solomon, 2005; Solomon, 1999). Since O mixing ratios are low, the chemical rate of change of O_x is nearly the same as the rate of change of ozone.

Odd oxygen is destroyed by several catalytic cycles. It is well known (e.g. Solomon, 1999) that the two dominant cycles in anthropogenic polar ozone depletion by halogens are the ClO dimer cycle (first proposed by Molina and Molina, 1987)
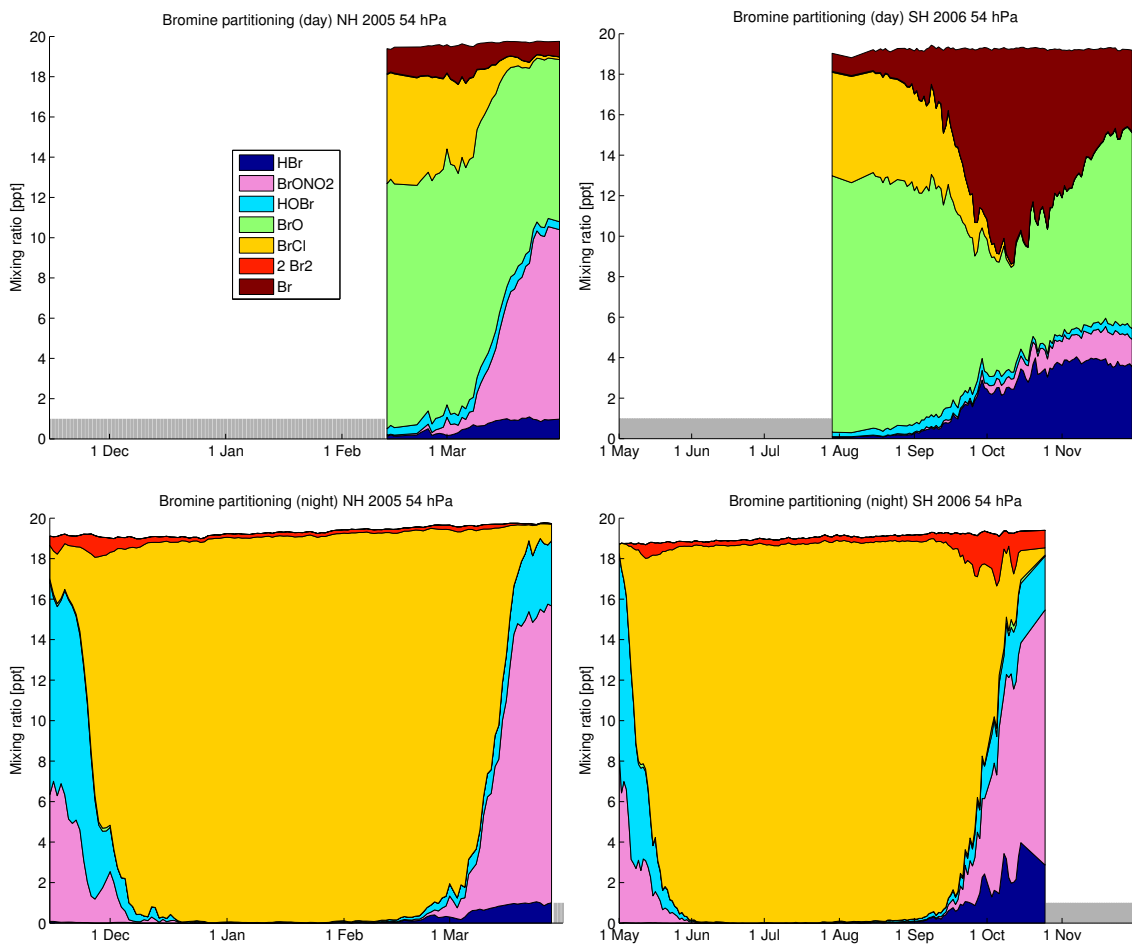
$$2\,(Cl + O_3 \rightarrow ClO + O_2\,) \tag{R29}$$

$$ClO + ClO + M \rightarrow Cl_2O_2 + M \tag{R30}$$

$$Cl_2O_2 + h\nu + M \rightarrow 2\,Cl + O_2 + M \tag{R31}$$

Figure 18. Vortex-averaged partitioning of inorganic bromine species for the Arctic winter 2004/2005 (left) and the Antarctic winter 2006 (right) at 54 hPa. Top row: Daytime averages (parts of the vortex where the solar zenith angle is smaller than 80°). Bottom row: Nighttime averages (parts of the vortex where the solar zenith angle is larger than 100°). Days without sufficient data for averaging are not shown (grey bars).
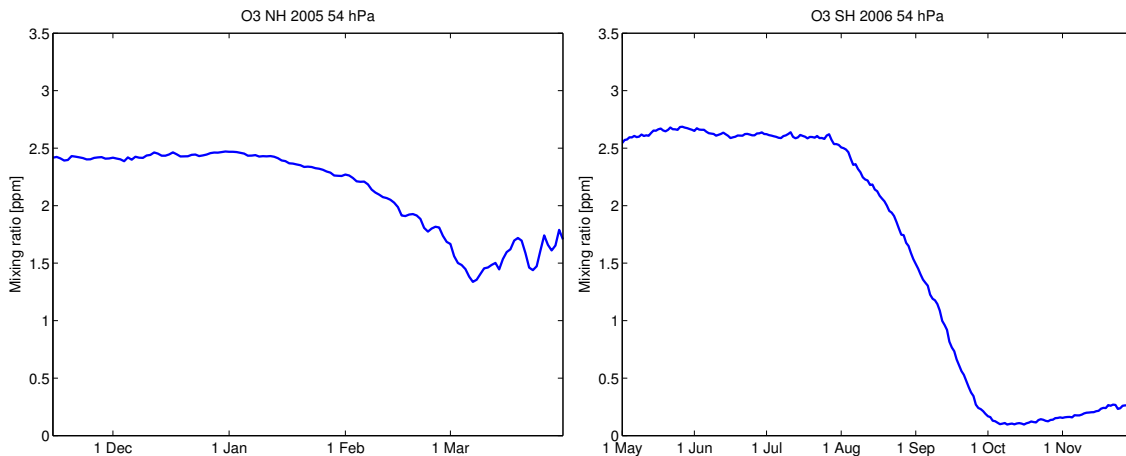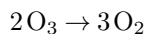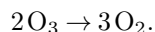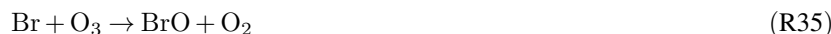
Figure 19. Vortex-averaged ozone mixing ratios for the Arctic winter 2004/2005 and the Antarctic winter 2006 at $54\,\mathrm{hPa}$.

$$2\,O_3 \rightarrow 3\,O_2$$

and the ClO–BrO cycle (first proposed by McElroy et al., 1986)

$$Cl + O_3 \rightarrow ClO + O_2 \hspace{4cm} \text{(R29)}$$

$$Br + O_3 \rightarrow BrO + O_2 \hspace{4cm} \text{(R35)}$$

$$\underline{BrO + ClO + M \rightarrow Br + Cl + O_2 + M} \hspace{2.4cm} \text{(R38)}$$

$$2\,O_3 \rightarrow 3\,O_2.$$

The ClO dimer cycle is effective ~~, because the~~ because Cl_2O_2 photolysis, which produces Cl and not ClO, is fast compared to the competing Cl_2O_2 loss reaction $Cl_2O_2 + M$ (Wayne et al., 1995, p. 2836). The uncertainty of the rate coeffcient of ~~the~~ Cl_2O_2 photolysis (R31) and the rate coefficient of the $BrO + ClO$ reaction (R38) are two of the parameters which produce the largest uncertainties with respect to ozone loss in models (e.g. Frieler et al., 2006; WMO, 2011), although much of the uncertainty in the photolysis rate coefficient has been resolved recently (Kawa et al., 2009; von Hobe and Stroh, 2012; Canty et al., 2016).

Figure 20 shows the contribution of the different catalytic cycles to the net chemical rate of change of ozone. For this purpose, the reaction rates of the rate limiting step of the reaction cycles have been used. This is possible here without ambiguities, since all rate limiting reactions are only involved in one cycle.

Typical peak loss rates vary between 40–60 ppb per day and are similar in both hemispheres in the altitude range $70\,\mathrm{hPa}$ to $32\,\mathrm{hPa}$ for these two winters (compare also the peak values of ClO_x discussed earlier and Figures 24, 72 of the supplement). Somewhat higher values of up to 70 ppb per day are only seen ~~in~~ at $42\,\mathrm{hPa}$ and $32\,\mathrm{hPa}$ in the southern hemisphere. Note however the underestimation of ClO in the southern hemisphere in ATLAS compared to MLS mentioned earlier. Hence,
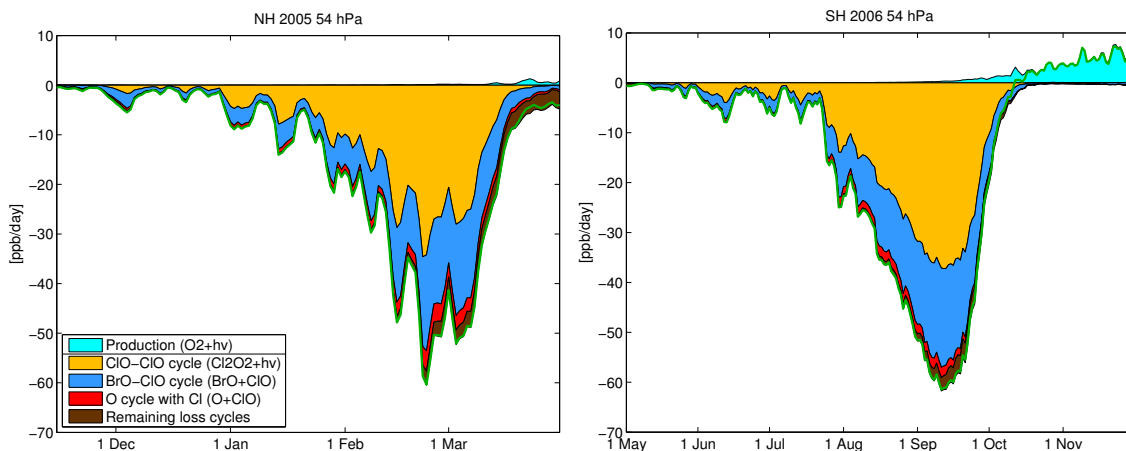
32

Figure 20. Vortex-averaged net chemical change of odd oxygen. The green line shows the net chemical change rate of ozone, which nearly equals the change rate of odd oxygen at this altitude. The contribution of different catalytic cycles to the ozone loss is shown by the reaction rates of their rate limiting step. Only the three most important cycles are shown, the contribution of other cycles is small. Ozone production, which is almost exclusively by the $O_2 + h\nu$ reaction, is shown in cyan.

the higher ozone depletion in the southern hemisphere is mainly caused by the much longer time period in which ClO_x is activated ~~in our model~~. Photochemical production of ozone is evident in March 2005 in the northern hemisphere and in October and November 2006 in the southern hemisphere and ~~increasing~~ increases with altitude (~~see~~ Figures 24, 48, 72, 96 of the supplement).

5   As long as appreciable amounts of ClO exist (January to February 2005 in the northern hemisphere, June to September 2006 in the southern hemisphere), the ClO–ClO cycle contributes about 50 % to the net ozone loss and the ClO–BrO cycle contributes about 30–40 % ~~in~~ at all altitudes (~~see~~ Figures 24, 48, 72, 96 of the supplement). These values compare well with the results of Kuttippurath et al. (2010) at 475 K ~~and~~ for 2005 (50% ClO–ClO to 30% ClO–BrO) and with the results of Frieler et al. (2006) (50% ClO–ClO to 30%–50% ClO–BrO, but for years different from 2005). See also Grenfell et al., 2006, for

10   case studies~~of the partitioning~~.

Loss cycles of the form

$$X + O_3 \rightarrow XO + O_2$$

$$\frac{XO + O \rightarrow X + O_2}{O + O_3 \rightarrow O_2 + O_2}$$
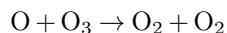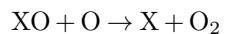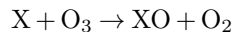
15   where ~~X = OH, H, NO, Cl, Br~~ $X = OH, H, NO, Cl$ or Br, which dominate in most latitudes and seasons, only play a minor role in the polar lower stratosphere due to the relatively low production of atomic oxygen by photolysis (e.g. von Hobe and Stroh, 2012). The ClO–O cycle contributes about 10 % at 54 hPa and increases in importance with altitude, in agreement with e.g. Kuttippurath et al. (2010).

33

The most important null cycle acting on odd oxygen apart from reactions R41 and R42 is the nitrogen cycle

$$O_3 + NO \rightarrow NO_2 + O_2 \hspace{4cm} (R6)$$

$$\underline{NO_2 + h\nu \rightarrow NO + O} \hspace{4cm} (R8)$$

$$O_3 \rightarrow O_2 + O.$$
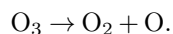
5   Interannual variability

In addition to the runs for the Arctic winter 2004/2005 and the Antarctic winter 2006, we performed model runs for the Arctic winter 2009/2010 and the Antarctic winter 2011 to get at least an idea of the interannual variability of the reaction rates and partitioning and to assess if the results can be generalized. Figures for the additional years can be found in the supplement.

Since meteorological conditions are usually very similar in the southern hemisphere from year to year, the results do not change significantly for the Antarctic winter 2011 compared to 2006, and the same discussion as for the winter 2006 applies. Except for rare cases, such as the vortex split in 2002, the dates, magnitudes of the values and the relative partitioning will also be applicable to other southern winters.

The northern winters 2004/2005 and 2009/2010 were taken as examples for a colder and a warmer winter, respectively, and reflect the larger meteorological variability in the northern hemisphere. The main differences are in the timing of the changes in reaction rates and mixing ratios. The first main difference is a later activation of chlorine (end of December ~~2010~~ 2009 compared to start of December ~~2005~~2004), reflected e.g. in the timing of the ~~heterogenous~~ heterogeneous reaction rates. The second main difference is an earlier deactivation by an earlier stratospheric warming in February. That means an earlier increase in e.g. $ClONO_2$, NO_x or HO_x and the associated reaction rates, and an earlier decrease in ClO_x. The timing of activation and deactivation can vary greatly between different northern winters, from winters with no chlorine activation ~~and~~ or heterogeneous ozone depletion at all to winters that stay cold until April and experience severe ozone loss (e.g. Santee et al., 2008).

The absolute values of the reaction rates and mixing ratios, the relative partitioning inside the chemical families and the relative importance of reactions remain similar for most species for these two northern winters. One of the notable exceptions is of course ozone, which shows less depletion in a warm winter like 2009/2010. This comparison suggests that the relative partitioning and the relative importance of reactions can be generalized to other northern winters, but that the absolute values of ozone depletion and of several reaction rates will differ.

6   Model validation

It is desirable that the results of the ATLAS model agree well with observations to increase the confidence in the model results for minor species and reaction rates which cannot be confirmed by observations. It is out of the scope of this study to give a comprehensive model validation against observations, but we include an extensive set of comparisons to observations of the MLS satellite instrument (e.g. Santee et al., 2008) and the ACE-FTS ~~satellite instruments~~ (Atmospheric Chemistry Experiment – Fourier Transform Spectrometer) satellite instrument (e.g. Bernath, 2017) in a supplement to provide additional information

for the interested reader. In addition, the reader is referred to Wohltmann et al. (2010) and Wohltmann et al. (2013) for a detailed validation.

Since there is reasonable agreement between measurements and the ATLAS model for many species, we will restrict discussion ~~on~~ to the notable differences between ATLAS and observations and show only some selected results in the main text. The focus is on a prominent disagreement between modeled mixing ratios of HCl and observations.

6.1   HCl discrepancy between model and measurements

Figure 21 and 22 show a comparison of the vortex-averaged mixing ratios of some important species (O_3, H_2O, HNO_3, HCl and N_2O, blue and black lines) with corresponding vortex averages measured by the MLS satellite instrument (e.g. Santee et al., 2008~~,~~) (red circles with bars for the accuracy, version 3 data, Livesey et al., 2011). Note that the vortex averages do not take into account the vortex tracer criterion (as in the preceding sections) to facilitate comparison with MLS (the supplement contains comparisons with MLS at individual locations for more detailed information). The blue lines denote the runs actually used in this paper (with a 5 K offset to HCl solubility), and the black lines denote the uncorrected model runs (without any change to HCl solubility).

It is obvious that the runs without a change to the HCl solubility significantly overestimate HCl, a behaviour also observed in other models like SD-WACCM (Brakebusch et al., 2013; Wegner, 2013; Solomon et al., 2015) or MIMOSA-CHIM (Kuttippurath et al., 2015). Interestingly, the SLIMCAT CTM shows a discrepancy of the same order of magnitude, but with the opposite sign in a recent publication (Santee et al., 2008), while in an older version, species mixing ratios depend on the model resolution (Chipperfield et al., 1997).

Apart from the discrepancy in HCl, the agreement of model and observations for other species like ozone, water vapour or HNO_3 is quite satisfactory. The reason for the HCl discrepancy is unknown, but several solutions are possible:

– The initial amount of $ClONO_2$ in the model is underestimated, which hinders the $HCl + ClONO_2$ reaction (discussed in Santee et al., 2008; Brakebusch et al., 2013; Wegner, 2013). $ClONO_2$ only represents about 30% of inorganic chlorine at the start of the winter and is clearly the limiting species of the reaction. An underestimation in ATLAS is however unlikely, since it is not supported by measurements of $ClONO_2$ by ACE-FTS (~~see~~ Figures 165, 167, ..., 171 of the supplement) and would require increasing the $ClONO_2$ mixing ratios by more than $100\,\%$.

– Less NO_x is transported across the vortex edge in the model compared to the real atmosphere, which impedes the reformation of $ClONO_2$ and HCl depletion via the $HCl + ClONO_2$ reaction (discussed in Solomon et al., 2015). This is likely very dependent on the transport and mixing scheme used in the model, and Eulerian (grid-based) models will show differences to Lagrangian (trajectory-based) models here due to the lower numerical diffusion in the latter. The underestimation of HCl in SLIMCAT (Santee et al., 2008) and the dependency of the species abundances on model resolution in the same model (Chipperfield et al., 1997) may point ~~into~~ in this direction.

While it cannot be excluded that less NO_x is transported across the vortex edge in ATLAS compared to the real atmosphere, the good agreement of most other species in ATLAS with measurements, including the tracer N_2O (Figure 21
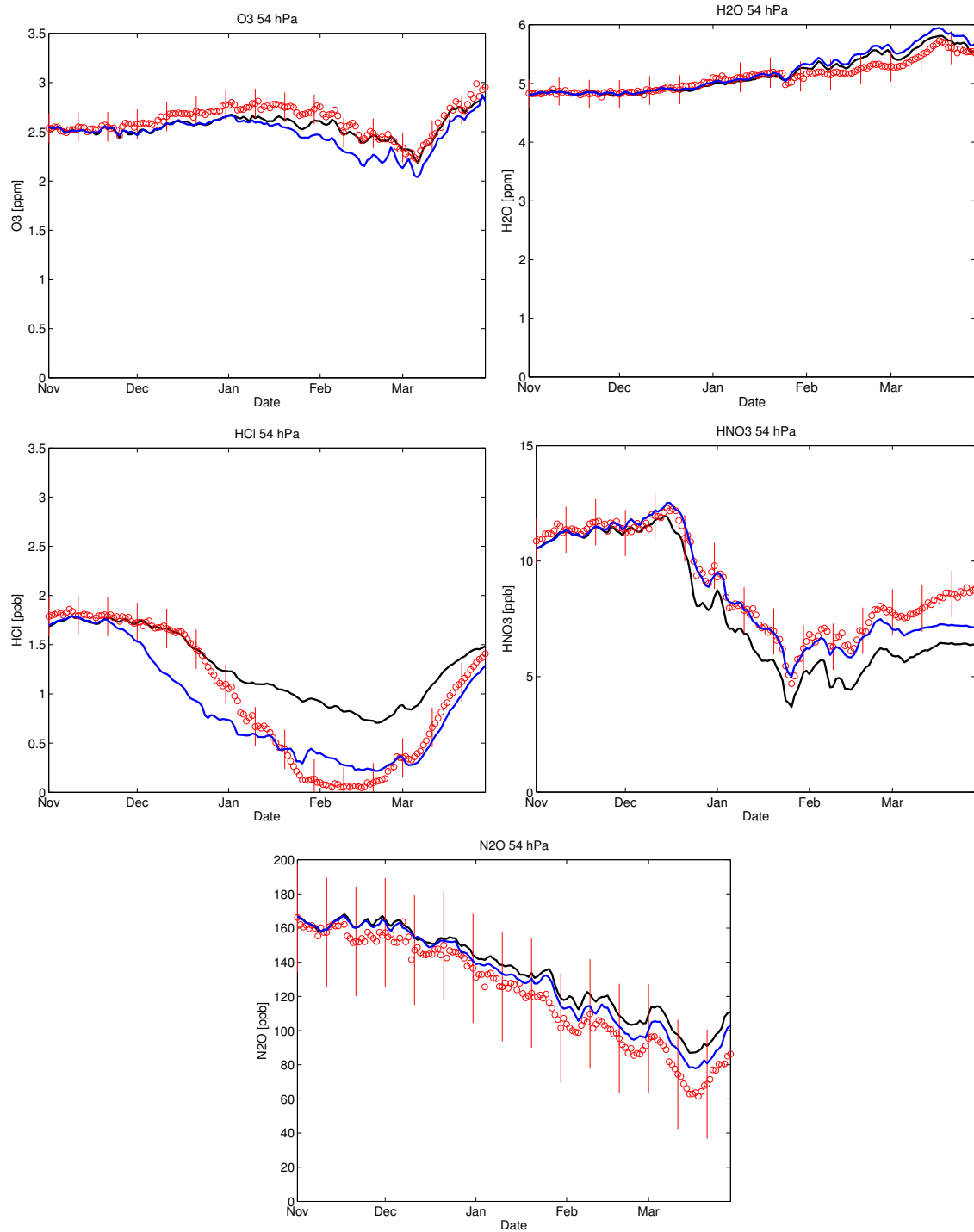
Figure 21. Vortex-averaged mixing ratios of O_3, H_2O, HCl~~and~~, HNO_3 and N_2O for the Arctic winter 2004/~~2005.~~ 2005 at 54 hPa. The red dots show MLS satellite measurements (version 3, with bars showing the accuracy), the blue lines show the ATLAS runs used in this paper and the black line shows the original runs which are not empirically corrected for the HCl discrepancy.
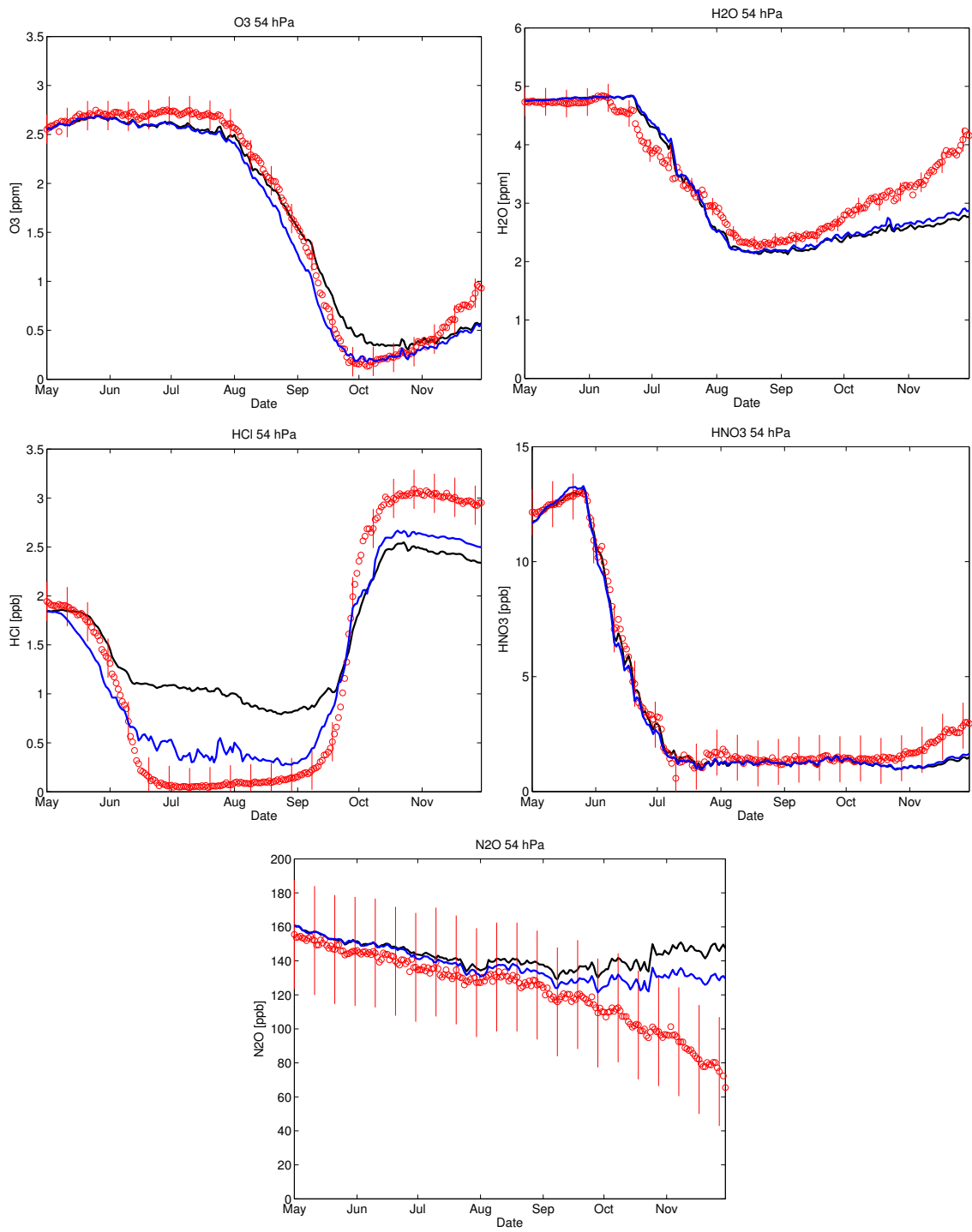
Figure 22. Comparison of vortex-averaged mixing ratios for the Antarctic winter 2006

and 22), suggests that this option is unlikely. As long as errors in subsidence do not compensate for errors in mixing, this also means that the HCl discrepancy cannot be caused by differences in subsidence between model and real atmosphere.

Note that there is a marked discrepancy in N_2O between MLS and the model in the southern hemisphere in October and November, which is however after the period of interest here. The reason for this discrepancy is unknown, but a possible reason could be overestimation of mixing across the vortex edge in ERA Interim in this time period.

- HCl is taken up in PSCs and sediments out of the observed layer (discussed in Wegner, 2013). This is not supported by either the temporal or the spatial evolution of HCl.

- An unknown heterogeneous reaction is depleting HCl. This cannot be excluded, but some boundary conditions need to be fulfilled, e.g. the reaction needs to involve HCl and it must not change the mixing ratios of other observed species too much.

- There is a temperature bias in the ERA Interim data compared to the real atmosphere or a water vapor bias in the model (discussed in Brakebusch et al., 2013; Wegner, 2013; Solomon et al., 2015). The solubility of HCl in STS droplets is a strong function of both temperature and water vapor. The discussion in Simmons et al. (2014) and our own comparisons at the station Ny Ålesund suggest that the bias between ERA Interim and radiosonde data is less than $0.3\,\mathrm{K}$ in the considered altitude range and cannot explain the differences between MLS and ATLAS. The water vapor data is in good agreement between MLS and ATLAS (Figure 21 and 22) and is also not likely to cause the differences in HCl.

- The parameterized solubility of HCl in STS droplets is underestimated (discussed in Brakebusch et al., 2013; Wegner, 2013). This is a promising possibility (since it does not affect most other species, consistent with the reasonable agreement of the other species to measurements), but it requires changes to the solubility that are ~~above~~ larger than the stated uncertainties of the solubility parameterization by Luo et al. (1995) that is used in the model.

Since there is not enough evidence to narrow down this list to a likely candidate, we decided on an empirical approach: We introduced a temperature offset for the calculation of the Henry constant of HCl and changed the offset until we obtained ~~a~~ good agreement between measured and modeled HCl, which was the case for an offset of $-5\,\mathrm{K}$. The effect of the changed Henry constant is twofold: First, it increases the amount of HCl dissolved in STS droplets. Second, it increases the rates of the heterogeneous reactions (even if only small amounts of HCl are dissolved) by changing the γ values. Brakebusch et al. (2013) and Solomon et al. (2015) did take the approach to introduce a ~~temperature bias~~ $-1.5\,\mathrm{K}$ temperature bias in the entire heterogeneous chemistry module, but we opted here for a different solution, since ~~introducing a temperature bias~~ this would have an additional direct temperature effect on reaction rates in the model.

The HCl mixing ratios of the model runs with the changed Henry constant agree considerably better than ~~before~~ those from the original runs with the satellite measurements in both hemispheres. ~~A larger discrepancy remains in December~~ However, there is a large underestimation of HCl in ATLAS now in December 2004 in the northern hemisphere. This causes chlorine activation to set in too early in December (similar to Santee et al., 2008), and there is an overestimation of peak ClO values of up to $0.5\,\mathrm{ppb}$ on 15 December (Figure 145 in the supplement). In the southern hemisphere, an overestimation of HCl by

ATLAS by about 0.2–0.4 ppb remains, which is roughly consistent with an underestimation of ClO in ATLAS of the same order of magnitude (Figures 153, 155, ..., 163 in the supplement).

In addition to the results for the corrected runs, the supplement shows the same figures for the uncorrected runs to assess the impact of the changes in HCl solubility. The main difference is considerably less chlorine activation in both hemispheres (e.g. the peak value of ~~ClO~~ ClO_x for the northern winter 2004/2005 at 54 hPa changes from 2.5 ppb to 1.5 ppb). This corresponds to higher mixing ratios of the reservoir gases and lower reaction rates of HCl and $ClONO_2$. In the northern hemisphere, the reduced chlorine activation leads to reduced ozone loss (e.g. the mixing ratio of ozone at 70 hPa at the end of March 2005 increases from 1 ppm to 1.5 ppm). However, in the southern hemisphere, chlorine activation is still sufficient to deplete ozone to near zero values. Most other findings remain largely unaffected, including: the relative importance of reactions, the relative partitioning and the results for the NO_x and HO_x chemistry.

6.2 Other notable differences

The supplement shows maps of comparisons to MLS satellite observations at 46 hPa for the northern winter 2004/2005 and the southern winter 2006. The maps show all measurements on the 15th of every month for the species ClO, HCl, H_2O, HNO_3, N_2O and O_3. Additonally, comparisons to ACE-FTS measurements are shown for the southern winter 2006 as a function of equivalent latitude and altitude. Species are H_2O, O_3, CH_4, HCl, $ClONO_2$, N_2O, NO, NO_2, N_2O_5 and HNO_3. In general, agreement is reasonable both for the spatial patterns and the absolute values, with the following exceptions:

- An underestimation of HNO_3 in both hemispheres outside of the vortex by the model compared to both MLS and ACE-FTS, which is however outside of the region of interest here and may be related to the initialization.

- An overestimation of O_3 outside of the vortex by the model, which may be related to the underestimation of HNO_3 (less ozone depletion by NO_x).

- A significant overestimation of $ClONO_2$ around 600 K by the model compared to ACE-FTS in the southern hemisphere, ~~very likely caused~~ which may be caused in part by the initialization (there is only a limited amount of measurements of $ClONO_2$ and initialization is based on a tracer relationship).

- NO_x is significantly overestimated by the model above 600 K in the southern hemisphere compared to ACE-FTS. This is however very difficult to interpret, since ACE-FTS measures only under high solar zenith angles, where the temporal change of the species is fast, which may lead to large errors in combination with the large satellite footprint.

7 Conclusions

We have given a quantitative analysis of the reactions involved in polar ozone depletion in the stratosphere. For clarity, this study focuses on vortex averages in a layer around 54 hPa for one specific winter in each hemisphere, with additional winters and pressure levels shown in a supplement. The chemistry of polar ozone depletion is well known, but quantitative estimates of

the partitioning of the chemical families or the importance of single reactions and reaction cycles are rare. To our knowledge, this is the first comprehensive study providing quantitative results averaged over the core of the polar vortex under conditions perturbed by heterogeneous chemistry. The main aim of this study is to quantify the partitioning of HO_x, NO_x and ClO_x, the relative importance of production and loss reactions and the timing of the reactions. Some selected findings are:

- Our results suggest that the relative partitioning ~~inside~~ within chemical families and the relative importance of reactions in the northern winter 2004/2005 and the southern winter 2006 can be generalized to other winters. The absolute values of ozone depletion, the absolute values of the reaction rates and the timing of changes will differ, particularly in the northern hemisphere.

- The ClO dimer cycle contributes about 50 % to the vortex-averaged ozone loss at 54 hPa in both hemispheres, while the ClO–BrO cycle contributes about 40 %, in good agreement with earlier studies (e.g. Frieler et al., 2006; Kuttippurath et al., 2010). The ClO–O cycle contributes about 10 % at 54 hPa and increases in importance with altitude at the expense of the ClO dimer and ClO–BrO ~~cycle~~cycles.

- In the southern hemisphere, there is a clear shift from chlorine activation by the $ClONO_2 + HCl$ reaction in early winter to activation by the $HOCl + HCl$ reaction later in winter. $HOCl + HCl$ accounts for about 70% of the activation of HCl in the southern hemisphere at 54 hPa in 2006 (integrated over time), while it accounts for only 30% of the activation in the northern hemisphere in 2005. The reason for this is the deactivation of chlorine by the reaction $Cl + CH_4$ in the southern hemisphere (caused in turn by the low ozone values), which provides HCl and produces HO_x (see e.g. Crutzen et al., 1992, Portmann et al., 1996). This can clearly be seen in rising HCl levels in September in the southern hemisphere and in increased HO_x levels.

- ClO_x peaks at 2.0 ppb at 70 hPa and at 2.5 ppb from 54hPa to 32 hPa in the northern hemisphere in both 2005 and ~~2010.~~ 2010 in the model. The peak values in the southern hemisphere in 2006 and 2011 are lower (2.0 ppb at 54 hPa and 42 hPa)~~due to less transport from above and less reactivation of than~~. There is however an underestimation of ClO of about 0.2–0.4 ppb compared to MLS in the southern hemisphere in ATLAS, consistent with an overestimation of HCl and an underestimation of chlorine activation, which is related to a difficulty to model HCl correctly in state-of-the-art CTMs (see below). Taking this into account, similar ClO_x levels are expected in the real atmosphere in both hemispheres. Under this assumption, our model results suggest that more transport of Cl_y from above in the northern hemisphere ~~. Hence, the~~ is countered by a more efficient activation of chlorine in the southern hemisphere. The higher ozone depletion in the southern hemisphere is mainly caused by the much longer time period in which ClO_x is activated in our model. About 70% of ClO_x is present as ClO during daytime at 54 hPa, in good agreement with e.g. Stimpfle et al. (2004).

- HO_x levels peak at 4 ppt. HO_x is mainly produced from CH_4 oxidation in the southern hemisphere, while in the northern hemisphere, production by HNO_3, CH_4 and H_2O play comparable roles. The partitioning between OH and HO_2 results in 20%–40% OH in the southern hemisphere and in 10%–20% OH in the northern hemisphere.

- NO_x levels are smaller than $2\,ppb$ in the northern hemisphere and smaller than $0.75\,ppb$ in the southern hemisphere due to the denitrified conditions there. The partitioning between NO and NO_2 during daytime results in $80\,\%$–$90\,\%$ NO in the southern hemisphere and $20\,\%$–$40\,\%$ NO in the northern hemisphere. The higher NO levels are caused by the much lower ozone levels in the southern hemisphere (e.g. Douglass et al., 1995).

- 60%–80% of the production of NO_x in spring is caused by the $HNO_3 + OH$ reaction at $54\,hPa$ in the northern hemisphere, the remainder is caused by the $HNO_3 + h\nu$ reaction (cf. Portmann et al., 1996). Deactivation of ClO_x by the formation of $ClONO_2$ in the northern hemisphere is caused by a shift in the fast equilibrium between ClO, NO_2 and $ClONO_2$, which in turn is caused by the production of NO_x (e.g. Portmann et al., 1996).

There was a significant discrepancy between the modelled and measured HCl mixing ratios in our original model runs, which has also been observed in other state-of-the-art models like SD-WACCM (Brakebusch et al., 2013; Wegner, 2013; Solomon et al., 2015), MIMOSA-CHIM (Kuttippurath et al., 2015) or SLIMCAT (Santee et al., 2008). The cause of these discrepancies in the different models is currently unknown. In the runs actually used in this paper, we apply an empirical correction based on changing the HCl solubility to bring the HCl mixing ratios in closer agreement to observations. However, a detailed discussion of this important issue comparing the different models would deserve its dedicated own study.

Results of this study are extensively used in a companion paper (Wohltmann et al., 2017) to develop a fast model for polar ozone chemistry.

References

Bernath, P. F.: The Atmospheric Chemistry Experiment (ACE), Journal of Quantitative Spectroscopy and Radiative Transfer, 186, 3–16, 2017.

Brakebusch, M., Randall, C. E., Kinnison, D. E., Tilmes, S., Santee, M. L., and Manney, G. L.: Evaluation of Whole Atmosphere Community Climate Model simulations of ozone during Arctic winter 2004–2005, J. Geophys. Res., 118, 2673–2688, doi:10.1002/jgrd.50226, 2013.

Brasseur, G. and Solomon, S.: Aeronomy of the Middle Atmosphere, D. Reidel Publishing Company, Dordrecht, 2005.

Brasseur, G., Orlando, J. J., and Tyndall, G. S., eds.: Atmospheric Chemistry and Global Change, Oxford University Press, New York, Oxford, 1999.

Burkholder, J. B., Orlando, J. J., and Howard, C. J.: Ultraviolet absorption cross sections of chlorine oxide (Cl_2O_2) between 210 and 410 nm, J. Phys. Chem., 94, 687–695, 1990.

Canty, T. P., Salawitch, R. J., and Wilmouth, D. M.: The kinetics of the ClOOCl catalytic cycle, J. Geophys. Res., pp. 13 768–13 783, doi:10.1002/2016JD025710, 2016.

Chapman, S.: A theory of upper-atmospheric ozone, Mem. Roy. Soc., 3, 103–125, 1930.

Chipperfield, M. P., Lutman, E. R., Kettleborough, J. A., Pyle, J. A., and Roche, A. E.: Model studies of chlorine deactivation and formation of $ClONO_2$ collar in the Arctic polar vortex, J. Geophys. Res., 102, 1467–1478, 1997.

Cohen, R. C., Wennberg, P. O., Stimpfle, M., Koplow, J., Anderson, J. G., Fahey, D. W., Woodbridge, E. L., Keim, E. R., Gao, R., Proffitt, M. H., Loewenstein, M., and Chan, K. R.: Are models of catalytic removal of O_3 by HO_x accurate? Constraints from in situ measurements of the OH to HO_2 ratio, Geophys. Res. Lett., 21, 2539–2542, 1994.

Crutzen, P. J., Müller, R., Brühl, C., and Peter, T.: On the potential importance of the gas phase reaction $CH_3O_2 + ClO \rightarrow ClOO + CH_3O$ and the heterogeneous reaction $HOCl + HCl \rightarrow H_2O + Cl_2$ in "ozone hole" chemistry, Geophys. Res. Lett., 19, 1113–1116, 1992.

Dee, D. P., Uppala, S. M., Simmons, A. J., Berrisford, P., Poli, P., Kobayashi, S., Andrae, U., Balmaseda, M. A., Balsamo, G., Bauer, P., Bechtold, P., Beljaars, A. C. M., van de Berg, L., Bidlot, J., Bormann, N., Delsol, C., Dragani, R., Fuentes, M., Geer, A. J., Haimberger, L., Healy, S. B., Hersbach, H., Hólm, E. V., Isaksen, L., Kållberg, P., Köhler, M., Matricardi, M., McNally, A. P., Monge-Sanz, B. M., Morcrette, J.-J., Park, B.-K., Peubey, C., de Rosnay, P., Tavolato, C., Thépaut, J.-N., and Vitart, F.: The ERA-Interim reanalysis: configuration and performance of the data assimilation system, Q. J. R. Meteorol. Soc., 137, 553–597, 2011.

Douglass, A. R., Schoeberl, M. R., Stolarski, R. S., Waters, J. W., III, J. M. R., Roche, A. E., and Massie, S. T.: Interhemispheric differences in springtime production of HCl and $ClONO_2$ in the polar vortices, J. Geophys. Res., 100, 13 967–13 978, 1995.

Fahey, D. W., Kelly, K. K., Kawa, S. R., Tuck, A. F., Loewenstein, M., Chan, K. R., and Heidt, L. E.: Observations of denitrification and dehydration in the winter polar stratospheres, Nature, 344, 321–324, 1990.

Farman, J. C., Gardiner, B. G., and Shanklin, J. D.: Large losses of total ozone in Antarctica reveal seasonal ClOx/NOx interaction, Nature, 315, 207–210, 1985.

Frieler, K., Rex, M., Salawitch, R. J., Canty, T., Streibel, M., Stimpfle, R. M., Pfeilsticker, K., Dorf, M., Weisenstein, D. K., and Godin-Beekmann, S.: Toward a better quantitative understanding of polar stratospheric ozone loss, Geophys. Res. Lett., 33, L10812, doi:10.1029/2005GL025466, 2006.

Grenfell, J. L., Lehmann, R., Mieth, P., Langematz, U., and Steil, B.: Chemical reaction pathways affecting stratospheric and mesospheric ozone, J. Geophys. Res., 111, D17311, doi:10.1029/2004JD005713, 2006.

Grooß, J.-U. and Russell III, J. M.: Technical note: A stratospheric climatology for O$_3$, H$_2$O, CH$_4$, NO$_x$, HCl and HF derived from HALOE measurements, Atmos. Chem. Phys., 5, 2797–2807, 2005.

Grooß, J.-U., Günther, G., Konopka, P., Müller, R., McKenna, D. S., Stroh, F., Vogel, B., Engel, A., Müller, M., Hoppel, K., Bevilacqua, R., Richard, E., Webster, C. R., Elkins, J. W., Hurst, D. F., Romashkin, P. A., and Baumgardner, D. G.: Simulation of ozone depletion in spring 2000 with the Chemical Lagrangian Model of the Stratosphere (CLaMS), J. Geophys. Res., 107, 8295, doi:10.1029/2001JD000456, 2002.

Hanisco, T. F.: Stratospheric chemistry and composition / HO$_x$, in: Encyclopedia of Atmospheric Sciences, edited by Holton, J. R., Curry, J. A., and Pyle, J. A., vol. 5, pp. 2174–2180, Academic Press, Elsevier, 2003.

Kawa, S. R., Stolarski, R. S., Newman, P. A., Douglass, A. R., Rex, M., Hofmann, D. J., Santee, M. L., and Frieler, K.: Sensitivity of polar stratospheric ozone loss to uncertainties in chemical reaction kinetics, Atmos. Chem. Phys., 9, 8651–8660, 2009.

Kremser, S., Schofield, R., Bodeker, G. E., Connor, B. J., Rex, M., Barret, J., Mooney, T., Salawitch, R. J., Canty, T., Frieler, K., Chipperfield, M. P., Langematz, U., and Feng, W.: Retrievals of chlorine chemistry kinetic parameters from Antarctic ClO microwave radiometer measurements, Atmos. Chem. Phys., 11, 5183–5193, 2011.

Kuttippurath, J., Godin-Beekmann, S., Lefèvre, F., and Goutail, F.: Spatial, temporal, and vertical variability of polar stratospheric ozone loss in the Arctic winters 2004/2005–2009/2010, Atmos. Chem. Phys., 10, 9915–9930, 2010.

Kuttippurath, J., Godin-Beekmann, S., Lefèvre, F., Santee, M. L., Froidevaux, L., and Hauchecorne, A.: Variability in Antarctic ozone loss in the last decade (2004–2013): high-resolution simulations compared to Aura MLS observations, Atmos. Chem. Phys., 15, 10 385–10 397, 2015.

Lait, L. R.: An alternative form for potential vorticity, J. Atmos. Sci., 51, 1754–1759, 1994.

Lary, D. J.: Gas phase atmospheric bromine photochemistry, J. Geophys. Res., 101, 1505–1516, 1996.

Lary, D. J., Chipperfield, M. P., Toumi, R., and Lenton, T.: Heterogeneous atmospheric bromine chemistry, J. Geophys. Res., 101, 1489–1504, 1996.

Lehmann, R.: Determination of dominant pathways in chemical reaction systems: An algorithm and its Application to Stratospheric Chemistry, J. Atmos. Chem., 41, 297–314, 2002.

Livesey, N. J., Read, W. G., Froidevaux, L., Lambert, A., Manney, G. L., Pumphrey, H. C., Santee, M. L., Schwartz, M. J., Wang, S., Cofeld, R. E., Cuddy, D. T., , Fuller, R. A., Jarnot, R. F., Jiang, J. H., Knosp, B. W., Stek, P. C., Wagner, P. A., and Wu, D. L.: Version 3.3 Level 2 data quality and description document, JPL D-33509, http://mls.jpl.nasa.gov, 2011.

Lowe, D. and MacKenzie, A. R.: Polar stratospheric cloud microphysics and chemistry, J. Atmos. Solar-Terr. Phys., 70, 13–40, 2008.

Luo, B., Carslaw, K. S., Peter, T., and Clegg, S. L.: Vapour pressures of H$_2$SO$_4$/HNO$_3$/HCl/HBr/H$_2$O solutions to low stratospheric temperatures, Geophys. Res. Lett., 22, 247–250, 1995.

McElroy, M. B., Salawitch, R. J., Wofsy, S. C., and Logan, J. E.: Reductions of Antarctic ozone due to synergistic interactions of chlorine and bromine, Nature, 321, 759–762, 1986.

Molina, L. T. and Molina, M. J.: Production of Cl$_2$O$_2$ from the self-reaction of the ClO radical, J. Phys. Chem., 91, 433–436, 1987.

Montzka, S. A.: Source gases that affect stratospheric ozone, in: Stratospheric Ozone Depletion and Climate Change, edited by Müller, R., chap. 2, pp. 33–77, RSC Publishing, Cambridge, 2012.

Müller, R., ed.: Stratospheric Ozone Depletion and Climate Change, RSC Publishing, Cambridge, 2012.

Nakajima, H., Wohltmann, I., Wegner, T., Takeda, M., Pitts, M. C., Poole, L. R., Lehmann, R., Santee, M. L., and Rex, M.: Polar Stratospheric Cloud evolution and chlorine activation measured by CALIPSO and MLS, and modelled by ATLAS, Atmos. Chem. Phys., 16, 3311–3325, 2016.

Peter, T. and Grooß, J.-U.: Polar Stratospheric Clouds and Sulfate Aerosol Particles: Microphysics, Denitrification and Heterogeneous Chemistry, in: Stratospheric Ozone Depletion and Climate Change, edited by Müller, R., chap. 4, pp. 108–144, RSC Publishing, Cambridge, 2012.

Pitts, M. C., Poole, L. R., Dörnbrack, A., and Thomason, L. W.: The 2009–2010 Arctic polar stratospheric cloud season: a CALIPSO perspective, Atmos. Chem. Phys., 11, 2161–2177, 2011.

Portmann, R. W., Solomon, S., Garcia, R. R., Thomason, L. W., Poole, L. R., and McCormick, M. P.: Role of aerosol variations in anthropogenic ozone depletion in the polar regions, J. Geophys. Res., 101, 22 991–23 006, 1996.

Sander, S. P., Abbatt, J., Barker, J. R., Burkholder, J. B., Friedl, R. R., Golden, D. M., Huie, R. E., Kolb, C. E., Kurylo, M. J., Moortgat, G. K., Orkin, V. L., and Wine, P. H.: Chemical kinetics and photochemical data for use in atmospheric studies, Evaluation Number 17, JPL Publication 10-06, Jet Propulsion Laboratory, California Institute of Technology, Pasadena, http://jpldataeval.jpl.nasa.gov, 2011.

Santee, M. L., MacKenzie, I. A., Manney, G. L., Chipperfield, M. P., Bernath, P. F., Walker, K. A., Boone, C. D., Froidevaux, L., Livesey, N. J., and Waters, J. W.: A study of stratospheric chlorine partitioning based on new satellite measurements and modeling, J. Geophys. Res., 113, doi:10.1029/2007JD009057, 2008.

Schofield, R., Frieler, K., Wohltmann, I., Rex, M., von Hobe, M., Stroh, F., Koch, G., Peter, T., Canty, T., Salawitch, R., and Volk, C. M.: Polar stratospheric chlorine kinetics from a self-match flight during SOLVE-II/EUPLEX, Geophys. Res. Lett., 35, L01807, doi:10.1029/2007GL031740, 2008.

Simmons, A. J., Poli, P., Dee, D. P., Berrisford, P., Hersbach, H., Kobayashi, S., and Peubey, C.: Estimating low-frequency variability and trends in atmospheric temperature using ERA-Interim, Q. J. R. Meteorol. Soc., 140, 329–353, 2014.

Solomon, S.: Stratospheric ozone depletion: A review of concepts and history, Rev. Geophys., 37, 275–316, 1999.

Solomon, S., Garcia, R. R., Rowland, F. S., and Wuebbles, D. J.: On the depletion of Antarctic ozone, Nature, 321, 755–758, 1986.

Solomon, S., Kinnison, D., Bandoro, J., and Garcia, R.: Simulation of polar ozone depletion: An update, J. Geophys. Res., 120, 7958–7974, doi:10.1002/2015JD023365, 2015.

Stimpfle, R. M., Wilmouth, D. M., Salawitch, R. J., and Anderson, J. G.: First measurements of ClOOCl in the stratosphere: The coupling of ClOOCl and ClO in the Arctic polar vortex, J. Geophys. Res., 109, D03301, doi:10.1029/2003JD003811, 2004.

Toon, O. B., Hamill, P., Turco, R. P., and Pinto, J.: Condensation of HNO_3 and HCl in the winter polar stratosphere, Geophys. Res. Lett., 13, 1284–1287, 1986.

von Hobe, M. and Stroh, F.: Stratospheric halogen chemistry, in: Stratospheric Ozone Depletion and Climate Change, edited by Müller, R., chap. 2, pp. 78–107, RSC Publishing, Cambridge, 2012.

von Hobe, M., Bekki, S., Borrmann, S., Cairo, F., D'Amato, F., Di Donfrancesco, G., Dörnbrack, A., Ebersoldt, A., Ebert, M., Emde, C., Engel, I., Ern, M., Frey, W., Griessbach, S., Grooß, J.-U., Gulde, T., Günther, G., Hösen, E., Hoffmann, L., Homonnai, V., Hoyle, C. R., Isaksen, I. S. A., Jackson, D. R., Jánosi, I. M., Kandler, K., Kalicinsky, C., Keil, A., Khaykin, S. M., Khosrawi, F., Kivi, R., Kuttippurath, J., Laube, J. C., Lefèvre, F., Lehmann, R., Ludmann, S., Luo, B. P., Marchand, M., Meyer, J., Mitev, V., Molleker, S., Müller, R., Oelhaf, H., Olschewski, F., Orsolini, Y., Peter, T., Pfeilsticker, K., Piesch, C., Pitts, M. C., Poole, L. R., Pope, F. D., Ravegnani, F., Rex, M., Riese, M., Röckmann, T., Rognerud, B., Roiger, A., Rolf, C., Santee, M. L., Scheibe, M., Schiller, C., Schlager, H., Siciliani de Cumis, M., Sitnikov, N., Søvde, O. A., Spang, R., Spelten, N., Stordal, F., Sumińska-Ebersoldt, O., Viciani, S., Volk, C. M., vom Scheidt, M., Ulanovski, A., von der Gathen, P., Walker, K., Wegner, T., Weigel, R., Weinbuch, S., Wetzel, G., Wienhold, F. G., Wintel, J., Wohltmann, I., Woiwode, W., Young, I. A. K., Yushkov, V., Zobrist, B., and Stroh, F.: Reconciliation of essential process parameters for an enhanced predictability of Arctic stratospheric ozone loss and its climate interactions, Atmos. Chem. Phys., 13, 9233–9268, 2013.

Waters, J. W., Froidevaux, L., Harwood, R. S., Jarnot, R. F., Pickett, H. M., Read, W. G., Siegel, P. H., Coeld, R. E., Filipiak, M. J., Flower, D. A., Holden, J. R., Lau, G. K., Livesey, N. J., Manney, G. L., Pumphrey, H. C., Santee, M. L., Wu, D. L., Cuddy, D. T., Lay, R. R., Loo, M. S., Perun, V. S., Schwartz, M. J., Stek, P. C., Thurstans, R. P., Chandra, K. M., Chavez, M. C., Chen, G.-S., Boyles, M. A., Chudasama, B. V., Dodge, R., Fuller, R. A., Girard, M. A., Jiang, J. H., Jiang, Y., Knosp, B. W., LaBelle, R. C., Lam, J. C., Lee, K. A., Miller, D., Oswald, J. E., Patel, N. C., Pukala, D. M., Quintero, O., Scaff, D. M., Snyder, W. V., Tope, M. C., Wagner, P. A., and Walch, M. J.: The Earth Observing System Microwave Limb Sounder (EOS MLS) on the Aura satellite, IEEE Transactions on Geoscience and Remote Sensing, 44, 1075–1092, 2006.

Wayne, R. P., Poulet, G., Biggs, P., Burrows, J. P., Cox, R. A., Crutzen, P. J., Hayman, G. D., Jenkin, M. E., Bras, G. L., Moortgat, G. K., Platt, U., and Schindler, R. N.: Halogen oxides: Radicals, sources and reservoirs in the laboratory and in the atmosphere, Atmos. Environ., pp. 2677–2881, 1995.

Wegner, T.: Chlorine activation and heterogenous chemistry in the polar stratosphere: Model simulations, in-situ- and satellite observations, Ph. D. thesis, University Wuppertal, http://elpub.bib.uni-wuppertal.de/servlets/DocumentServlet?id=3573, 2013.

WMO: World Meteorological Organization (WMO) / United Nations Environment Programme (UNEP), Scientific assessment of ozone depletion: 2010, Global Ozone Research and Monitoring Project – Report No. 52, 2011.

Wohltmann, I. and Rex, M.: The Lagrangian chemistry and transport model ATLAS: validation of advective transport and mixing, Geosci. Model Dev., 2, 153–173, 2009.

Wohltmann, I., Lehmann, R., and Rex, M.: The Lagrangian chemistry and transport model ATLAS: simulation and validation of stratospheric chemistry and ozone loss in the winter 1999/2000, Geosci. Model Dev., 3, 585–601, 2010.

Wohltmann, I., Wegner, T., Müller, R., Lehmann, R., Rex, M., Manney, G. L., Santee, M. L., Bernath, P., Sumińska-Ebersoldt, O., Stroh, F., von Hobe, M., Volk, C. M., Hösen, E., Ravegnani, F., Ulanovsky, A., and Yushkov, V.: Uncertainties in modelling heterogeneous chemistry and Arctic ozone depletion in the winter 2009/2010, Atmos. Chem. Phys., 13, 3909–3929, 2013.

Wohltmann, I., Lehmann, R., and Rex, M.: Update of the Polar SWIFT model for polar stratospheric ozone loss (Polar SWIFT version 2), Geophys. Model Dev., 10, 2671–2689, 2017.